Formation of a PSI–PSII megacomplex containing LHCSR and PsbS in the moss *Physcomitrella patens*

Ryo Furukawa[1], Michiki Aso[1], Tomomichi Fujita[2], Seiji Akimoto[3], Ryouichi Tanaka[1], Ayumi Tanaka[1], Makio Yokono[1,4]*, and Atsushi Takabayashi[1]*

[1]Institute of Low-Temperature Science, Hokkaido University, N19 W8 Kita-Ku, Sapporo 060-0819, Japan

[2]Faculty of Science, Hokkaido University, N10 W8 Kita-ku, Sapporo 060-0810, Japan

[3]Graduate School of Science, Kobe University, Kobe 657-8501, Japan

[4]Innovation Center, Nippon Flour Mills Co., Ltd., Atsugi 243-0041, Japan

*Co-Corresponding authors.

E-mail: filia@mac.com, TEL: +81-80-3295-1623

E-mail: takabayashi@pop.lowtem.hokudai.ac.jp, TEL: +81-11-706-5493

Acknowledgments

This work was supported by JSPS (Japan Society for the Promotion of Science) KAKENHI Grant Numbers 23770035 to A. Takabayashi, 16H06553 to S. Akimoto, and 16H06554 to R. Tanaka.

Conflict of interest

The authors declare that they have no conflict of interest.

Abstract

Mosses are one of the earliest land plants that diverged from fresh-water green algae. They are considered to have acquired a higher capacity for thermal energy dissipation to cope with dynamically changing solar irradiance by utilizing both the “algal-type” light-harvesting complex stress-related (LHCSR)-dependent and the “plant-type” PsbS-dependent mechanisms. It is hypothesized that the formation of photosystem (PS) I and II megacomplex is another mechanism to protect photosynthetic machinery from strong irradiance. Herein, we describe the analysis of the PSI–PSII megacomplex from the model moss, *Physcomitrella patens*, which was resolved using large-pore clear-native polyacrylamide gel electrophoresis (lpCN-PAGE). The similarity in the migration distance of the *Physcomitrella* PSI–PSII megacomplex to the Arabidopsis megacomplex shown during lpCN-PAGE suggested that the *Physcomitrella* PSI–PSII and Arabidopsis megacomplexes have similar structures. Time-resolved chlorophyll fluorescence measurements show that excitation energy was rapidly and efficiently transferred from PSII to PSI, providing evidence of an ordered association of the two photosystems. We also found that LHCSR and PsbS co-migrated with the *Physcomitrella* PSI–PSII megacomplex. The megacomplex showed pH-dependent chlorophyll fluorescence quenching, which may have been induced by LHCSR and/or PsbS proteins with the collaboration of zeaxanthin. We discuss the mechanism that regulates the energy distribution balance between two photosystems in *Physcomitrella*.

Keywords *Physcomitrella*, PSI–PSII megacomplex, LHCSR, CN-PAGE

55 **Introduction**

56 Plants contain photosystems that absorb light energy and transfer it to the reaction center to
57 drive photosynthetic electron transfer. Oxygenic photosynthesis requires the co-operative work of two
58 photosystems (PSI and PSII); therefore, the regulation of excitation energy distribution between PSI and
59 PSII is important to enable plants to avoid photooxidative damage (Minagawa and Tokutsu 2015; Niyogi
60 and Truong 2013; Ruban 2015; Xu et al. 2015; Wobbe et al. 2016). Therefore, rapid mechanisms for the
61 fine-tuning of energy distribution between these two photosystems are essential for adaption to terrestrial
62 environments, where the intensity of sunlight dynamically fluctuates, even over the short term (Minagawa
63 and Tokutsu 2015; Ruban 2015; Xu et al. 2015). One such mechanism is non-photochemical quenching
64 (NPQ), which enables PSII to dissipate excess light energy harmlessly as heat (Goss and Lepetit 2015;
65 Minagawa and Tokutsu 2015; Niyogi and Truong 2013; Ruban 2015, 2016; Wobbe et al. 2016; Xu et al.
66 2015). NPQ is induced and relaxed, depending on the pH gradient across thylakoid membranes, from
67 within seconds to minutes. State transition during photosynthesis is another mechanism that rapidly
68 regulates the excitation energy distribution between the two photosystems by the reversible allocation of
69 the light-harvesting complex II (LHCII) between them (Minagawa and Tokutsu 2015; Wobbe et al. 2016;
70 Xu et al. 2015). This transition is regulated by the phosphorylation of mobile LHCII, which is performed
71 by redox-active kinases (Bellafiore et al. 2005; Pesaresi et al. 2009). The induction and relaxation of the
72 state transition can also occur within minutes.

In addition to NPQ and state transition, the spillover of excitation energy between the two photosystems can contribute to the regulation of the balance of energy distribution between them. First, Järvi et al. (2011) reported the presence of large protein complexes comprising both PSI and PSII in *Arabidopsis thaliana* (hereafter Arabidopsis). Additionally, Yokono et al. (2015) provided spectrochemical evidence showing that the excitation energy can be shared between the two photosystems in the Arabidopsis PSI–PSII megacomplexes. It is also hypothesized that the megacomplex is formed in the marginal region of the appressed grana membranes, where PSI and PSII are present (Suorsa et al. 2014). In addition to Arabidopsis, PSI–PSII megacomplex formation was also reported in an early-branched vascular plant *Selaginella martensii* (Ferroni et al. 2016) and a green alga *Neochloris oleoabundans* (Giovanardi et al. 2017). Furthermore, the spillover from PSII to PSI can be observed in a wide variety of green plants, including green algae (Yokono et al. 2019). These findings showed that the spillover within the PSI–PSII megacomplex occur widely in the green lineage. The amount of the PSI–PSII megacomplex may rapidly change, depending on light conditions, which contributes to the regulation of energy distribution between PSI and PSII (Ferroni et al. 2016; Suorsa et al. 2015; Yokono et al. 2015).

The moss, *Physcomitrella patens* (Hedw.) (hereafter *Physcomitrella*), is a model plant for understanding the evolutionary changes in photosystems from green algae to land plants. It belongs to an early terrestrial group in the green lineage and displays photosynthetic regulation characteristics

intermediate between green algae and higher plants (Niyogi and Truong 2013). Specifically, *Physcomitrella* possesses both PsbS- and LHCSR-dependent NPQ (Iwai and Yokono 2017; Niyogi and Truong 2013; Peers et al. 2009). To date, PsbS- and LHCSR-dependent NPQ have been reported in the green lineage (Niyogi and Truong 2013; Peers et al. 2009). Higher plants only possess PsbS-dependent energy-dependent (qE) quenching because they have lost the LHCSR protein during evolution (Niyogi and Truong 2013). Although green algae possess both PsbS- and LHCSR-dependent NPQ, LHCSR-dependent NPQ is the primary NPQ in green algae. A recent study (Correa-Galvis et al. 2016) reported that *Chlamydomonas reinhardtii* (hereafter Chlamydomonas) PsbS is required to activate the LHCSR-dependent NPQ, suggesting that PsbS works cooperatively with LHCSR in green algae. In contrast, in *Physcomitrella*, the sub-thylakoid localization of PsbS is different from that of LHCSR (Pinnola et al. 2015). A single loss of PsbS or LHCSR leads to a similar decrease in NPQ, while the simultaneous loss of PsbS and LHCSR proteins reduced NPQ to almost zero (Alboresi et al. 2010; Gerotto et al. 2011). In addition, the mutant plants lacking both PsbS and LHCSR were more susceptible to high light intensities than the single mutant (Alboresi et al. 2010). These data showed that both PsbS and LHCSR have an essential role in NPQ in *Physcomitrella*. In this sense, *Physcomitrella* has an intermediate characteristic for the NPQ that is different from green algae and higher plants. Furthermore, *Physcomitrella* has a strong capacity to dissipate excess light energy as heat, because both PsbS- and LHCSR-dependent NPQ

occurred additively (Alboresi et al. 2010). This should contribute to the early adaptation to the strong and fluctuating light conditions in the terrestrial environment (Alboresi et al. 2010).

In the present study, we demonstrate the presence of the PSI–PSII megacomplex in the protonemata of *P. patens*, which can share excitation energy between the two photosystems. The megacomplex possesses low-energy chlorophylls in PSI-LHCI, similar to higher plants (Yokono et al. 2015). Low-energy chlorophylls can mediate $P700^+$ quenching (Croce and van Amerongen 2013) and may possibly mediate zeaxanthin-dependent quenching (Ballottari et al. 2014). In addition, the megacomplex showed a pH-dependent quenching ability, most likely due to its interaction with LHCSR and PsbS, which can contribute to the early adaptation to the strong and fluctuating light conditions in the terrestrial environment.

Material and methods

Plant materials

P. patens protonemata were cultured on a layer of cellophane overlaid on BCDAT (BCD medium (Nishiyama et al. 2000) supplemented with 1 mM $CaCl_2$ and 5 mM di-ammonium [+]-tartrate) solidified with 0.8% (w/v) agar at 25 °C under continuous light (40 μmol photons m^{-2} s^{-1}). Four-day-old cultured protonemata were used as the low-light sample. Several of the 4-day-old cultured protonemata were

125 further illuminated with strong light (500 µmol photons m^{-2} s^{-1}) for 1 h with cold spot fiber optics (PCS-

126 UMX250, NPI, Tokyo, Japan), and were used as the strong light sample.

127

128 **Isolation of thylakoid membranes**

129 The isolation of thylakoid membranes was performed largely according to the method described by Järvi

130 et al. (2011). All procedures were performed on ice or at 4 °C. The protonemata were suspended in a

131 grinding buffer (50 mM Hepes/KOH (pH 7.5), 330 mM sorbitol, 2 mM EDTA, 1 mM $MgCl_2$, 5 mM

132 ascorbate, 0.05% BSA, 10 mM sodium fluoride, and 0.25 mg mL^{-1} Pefabloc (Sigma-Aldrich, St. Louis,

133 MO, USA)). Approximately 1 mL of the suspension was transferred to a 2 mL vial containing 1 g of glass

134 beads (0.5 mm diameter) and the protonemata were disrupted by three × 10 s-disruption treatments using

135 a Mini-Bead Beater (Waken B Tech Co., Ltd, Kyoto, Japan). The homogenate was immediately

136 centrifuged at 5,000 × *g* for 4 min at 4 °C and resuspended in a shock buffer (50 mM Hepes/KOH (pH

137 7.5), 5 mM sorbitol, 5 mM $MgCl_2$, and 10 mM sodium fluoride). After centrifugation at 5,000 × *g* for 4

138 min at 4°C, the pellet was resuspended in a storage buffer (50 mM Hepes/KOH (pH 7.5), 100 mM

139 sorbitol, 10 mM $MgCl_2$, and 10 mM sodium fluoride) at a concentration of 1.5 mg mL^{-1} chlorophyll.

140

141 **Clear-native (CN)-PAGE**

142 CN-PAGE was performed in accordance with the methodology used by Umetani et al. (2018). The
143 isolated thylakoid membranes were resuspended in a solubilization buffer (50 mM imidazole/HCl (pH
144 7.0), 20% glycerol, 5 mM 6-aminocaproic acid, and 1 mM EDTA). An equal volume of 2% α-dodecyl
145 maltoside (DM) and 0.01-volumes of protease inhibitor cocktail (Sigma-Aldrich, St. Louis, MO, USA)
146 were added to the resuspended thylakoids and the chlorophyll-protein complexes were solubilized on ice
147 for 1 min. Insoluble material was removed from the samples by centrifugation at 21,600 × *g* at 4 °C for 1
148 min. After the addition of a 0.5-volumes of 20 mg mL^{-1} amphipol A8-35 (Anatrace, OH, USA) to the
149 supernatant, the samples were separated on 4%–13% polyacrylamide gradient gels at 4 °C using an anode
150 buffer (50 mM imidazole/HCl (pH 7.0 at 4 °C)) and a cathode buffer (50 mM Tricine and 15 mM
151 imidazole/HCl (pH 7.0 at 4 °C)).
152
153 **Large-pore (lp)CN-PAGE**
154 The lpCN-PAGE was performed using the procedure described by Järvi et al. (2011). A 25BTH20G
155 buffer (25 mM BisTris/HCl (pH 7.0), 20% (w/v) glycerol, and 0.25 mg mL^{-1} Pefabloc) was added to the
156 thylakoid membrane suspension to achieve a concentration of 1 mg mL^{-1} chlorophyll. To solubilize the
157 thylakoid protein complexes with digitonin, an equal volume of 2% digitonin in the 25BTH20G buffer
158 was added to the thylakoid suspension and incubated at 20 °C in the dark for 5 min with continuous
159 stirring. After centrifugation to remove insoluble materials, a 1/6 volume of 20 mg mL^{-1} amphipol A8-35

160 (Anatrace, OH, USA) was added to the supernatant. The samples were loaded onto lpCN gels
161 immediately after the solubilization process. The separation gels contained 3.5%–13% (w/v)
162 polyacrylamide, which is composed of acrylamide and bisacrylamide in the ratio of 29:1. The sample gels
163 contained 3% polyacrylamide, which is composed of acrylamide and bisacrylamide in a ratio of 4:1.
164 Electrophoresis was performed using an anode buffer (50 mM BisTris/HCl (pH 7.0 at 4 °C)) and a
165 cathode buffer (50 mM Tricine, 15 mM BisTris/HCl (pH 7.0 at 4 °C), and 0.01% amphipol A8-35).
166
167 **Two-dimensional lpCN/SDS-PAGE**
168 Two-dimensional (2D)-lpCN/SDS-PAGE was performed using the procedure described by Umetani et al.
169 (2018). Proteins in an lpCN-PAGE gel strip were denatured in a solubilization buffer (1% SDS and 1% 2-
170 mercaptoethanol) for 60 min at 30 °C and separated on a 14% acrylamide gel containing 4 M urea, using
171 the Laemmli system. Silver-staining was performed using the Pierce Silver Stain kit (ThermoFisher
172 Scientific, Rockford, IL, USA), according to the manufacturer's instructions.
173
174 **Immunoblotting**
175 The separated proteins were transferred to a polyvinylidene fluoride membrane (PolyScreen PVDF
176 transfer membrane, PerkinElmer Life Sciences, MA, USA) and detected by using specific antibodies and
177 a Western Lightning Plus-ECL (PerkinElmer Life science, MA, USA). All antibodies used in the present

178 study were purchased from Agrisera (Vännäs, Sweden). Anti-PsbB (AS04 038) and anti-PsbC antibodies
179 (AS11 1787) were used for detection of PSII core subunits. Anti-PsaD antibodies (AS09 461) were used
180 to detect a core subunit of PSI. Anti-Lhcb2 (AS01 003) and Lhcb3 (AS01 002) antibodies were used to
181 detect the major LHCII proteins. Anti-LHCSR1 antibodies (AS15 3081) were used for the detection of an
182 LHCSR protein.
183
184 **Spectroscopic analyses**
185 Time-resolved fluorescence measurements and analysis were performed at pH 7 and pH 4.5 by using the
186 PSI–PSII megacomplexes from the control and the 1 h-strong light illuminated plants, as described by
187 Yokono et al. (2015). The PSI–PSII megacomplex in the lpCN gel was soaked for 5 min at 4 °C using a
188 buffer containing 50 mM BisTris/HCl (pH 7 or pH 4.5) and 0.5 M 6-aminocaproic acid. The excitation
189 wavelength was 408 nm and the repetition rate was 2 MHz, which did not interfere with measurements up
190 to 100 ns (24.4 ps per channel × 4,096 channels). To improve the time resolution, time-resolved
191 fluorescence was also measured up to 10 ns (2.4 ps per channel × 4,096 channels). After a global analysis
192 of the fluorescence kinetics, fluorescence decay-associated spectra were constructed. Steady-state
193 fluorescence spectra were measured by using an F-2500 spectrophotometer (Hitachi). The optical slit
194 widths for excitation and emission were 10 and 2.5 nm, respectively. Steady-state absorption spectra at

195 room temperature (20 °C–25 °C) were measured based on the methodology described by Umetani et al.
196 (2018).
197
198 **Pigment Determination**
199 To extract pigments, *Physcomitrella* protonemata cells were homogenized in acetone with stainless beads
200 (5 mm in diameter, TCS0-0100, Bio medical science, Tokyo) for 1 min using the ShakeMaster bead
201 shaker (BioMedical Science Co. Ltd, Tokyo, Japan). The homogenates were centrifuged at 21,600 × g for
202 5 min, and the supernatant was loaded onto a C18 column (YMC AL303 250 × 4.6 mm, 5 μm, YMC Co.,
203 Ltd., Kyoto, Japan). The sample was eluted with an isocratic flow of solvent A (100% methanol) for 17
204 min, followed by a linear gradient from solvent A to B (60% methanol, 20% ethanol, 20% hexane) in 5
205 min and with an isocratic flow of solvent B at a flow rate of 0.8 ml/min. The eluates were monitored by a
206 L-2450 photodiode array detector (HITACHI High Technologies Science Corporation, Tokyo, Japan) at
207 450 nm. The pigments were identified and quantified by comparing their absorption spectra with relevant
208 standard pigments.
209
210 **Results**
211 **Isolation of a *Physcomitrella* PSI–PSII megacomplex by lpCN-PAGE**

212 The PSI–PSII megacomplex is one of the largest known plant complexes and is estimated to be larger
213 than 3,000 kDa (calculated based on the structural model of the Arabidopsis megacomplex in Yokono et
214 al. 2019). Only a few techniques currently exist that can resolve the size of the complex—such as size-
215 exclusion chromatography and sucrose-density gradient centrifugation. To the best of our knowledge,
216 only native PAGE systems have been successful in resolving the PSI–PSII megacomplex thus far (Ferroni
217 et al. 2016; Giovanardi et al. 2017; Järvi et al. 2011; Yokono et al. 2015). Moreover, standard blue-
218 native (BN) and clear-native (CN)-PAGE systems cannot be used to isolate the PSI–PSII megacomplex
219 because it is too large to enter the separation gel and must, therefore, remain in the sample gel (Järvi et al.
220 2011). Therefore, for this study, we used large-pore CN-PAGE (lpCN-PAGE)—a process that consists of
221 using large-pore acrylamide gel that allows the separation of the megacomplex from the rest of the
222 photosynthetic complexes and the insolubilized thylakoid membranes.
223 We began by solubilizing the thylakoid protein complexes using digitonin from cells grown
224 under low-light conditions and from cells illuminated with strong light for 1 h. DOC is typically used to
225 provide the negative charge required to separate the solubilized protein complexes by lpCN-PAGE at a
226 neutral pH. However, we replaced DOC with amphipol A8-35 for this study.
227 Amphipols are a new class of amphipathic polymer that enable protein complexes to enhance
228 their stability in detergent-free solutions. Amphipol A8-35, in particular, has been widely used in the
229 stabilization of membrane proteins (Popot et al. 2011; Watanabe et al. 2019). As a result of using this

technique, we succeeded in resolving several pigment-protein complexes (Fig. 1). As far as we know, this is the first study demonstrating the use of lpCN-PAGE using amphipols. Based on 2D-lpCN/SDS-PAGE, immunoblotting analysis (Fig. 2), and silver-staining (Fig. S1), the three major pigment-protein bands resolved by lpCN-PAGE were identified as a PSI–PSII megacomplex, a PSI-LHCI and PSII dimer, and an LHCII trimer, respectively. The PSII-LHCII was not clearly observed, because the grana core where the PSII-LHCII is mostly localized, is only partially solubilized by digitonin. Passing the PSI–PSII megacomplex band through the sample gel during lpCN-PAGE showed that it was a protein complex rather than insufficiently solubilized membrane particles. The *Physcomitrella* PSI–PSII megacomplex contained PSI, PSII, and LHCII proteins (Fig. 2), as found in the Arabidopsis megacomplex (Yokono et al. 2015). The molecular weights of the PSI-LHCI and PSII dimer were typically quite similar, which resulted in similar migration distances (Fig. 1). Smaller PSI–PSII complexes, which had similar migration distances, might be present in the band (Yokono et al. 2015), although no further analysis was conducted in the present study.

Recently, we reported a structural model of the Arabidopsis PSI–PSII megacomplex, based on the negatively-stained particles observed by electron microscopy (Yokono et al. 2019). In this model, one PSII dimer was sandwiched by two PSI-LHCI complexes with two-fold rotational symmetry, and additional LHCII trimers surrounded peripherally. If the *Physcomitrella* PSI–PSII megacomplex had a similar structure to this model, its molecular size should be similar to that of the Arabidopsis

megacomplex. To compare the molecular sizes of the *Physcomitrella* PSI–PSII megacomplex and the Arabidopsis megacomplex, we resolved the digitonin-solubilized thylakoid protein complexes from Arabidopsis and *Physcomitrella* by lpCN-PAGE using different acrylamide concentrations (3%–13% and 3.25%–13%) (Fig. 3). The subunit compositions of the *Physcomitrella* PSI–PSII megacomplexes resolved by the two different gels [3.5%–13% (Fig 1) and 3.25%–13% (Fig. 3)] appeared almost identical, based on the silver-stained 2D-lpCN/SDS-PAGE (Figs. S1, S2). The green band, other than the PSI–PSII megacomplex, did not appear around it even when the gel concentrations were altered (Figs. 1, 3). This supports the hypothesis that band contamination, such as PSII-LHCII megacomplexes, was negligible. On the other hand, the PSI–PSII megacomplex band appeared somewhat smeared (Figs. 1, 3). This is most likely due to the structural heterogeneity of the megacomplex, which includes the varied binding patterns of peripheral LHCIIs to the PSI–PSII megacomplex as shown and discussed by Yokono et al. (2019). The migration distances of the *Physcomitrella* PSI–PSII megacomplexes were similar to those of Arabidopsis, which demonstrated that the molecular mass of the PSI–PSII megacomplexes in Arabidopsis and *Physcomitrella* were similar to each other (Fig. 3). These data suggested that the structure of the *Physcomitrella* PSI–PSII megacomplex is similar to that of the Arabidopsis PSI–PSII megacomplex.

LHCSR is involved in the NPQ formation of both PSI and PSII in *Physcomitrella*, though the protein is localized in the stroma lamellae and grana margin, where PSII is scarcely distributed (Pinnola et al. 2015). As the PSI–PSII megacomplex likely localizes in the stroma lamellae, we hypothesized that

LHCSR binds to the PSI–PSII megacomplex and dissipates the absorbed energy as heat. To verify this hypothesis, we further performed immunoblotting analysis of LHCSR after 2D-lpCN/SDS-PAGE using anti-LHCSR antibodies (Fig. 2). The results showed that LHCSR co-migrated in the PSI–PSII megacomplex, in addition to their monomeric form, suggesting that the *Physcomitrella* PSI–PSII megacomplex contained LHCSR. As LHCSR has been lost in higher plants during plant evolution, the presence of LHSCR in the PSI–PSII megacomplex represents a significant difference in the PSI–PSII megacomplexes of *Physcomitrella* and Arabidopsis. In addition, the immunoblotting analysis (Fig. S3) showed that PsbS co-migrated with the PSI-PSII megacomplex as well in our lpCN-PAGE analysis. The results are consistent with a previous report showing the co-migration of PsbS and the PSI-PSII megacomplex in Arabidopsis (Suorsa et al. 2015). The presence of both LHCSR and PsbS proteins in the PSI-PSII megacomplex implies that they might contribute to dissipating the excess energy in the megacomplex as heat.

Steady-state fluorescence emission spectra of the PSI–PSII megacomplex at 77 K

The PSI–PSII megacomplex separated by lpCN-PAGE (Fig. 1) was further characterized by its steady-state fluorescence emission spectra at 77 K (Fig. 4). Because the individual fluorescence emission spectra of the PSI-LHCI, the PSII-LHCII, and the LHCII trimer are required to analyze the PSI–PSII megacomplex as references, we solubilized the thylakoid protein complexes by α-DM and resolved them

284 with a CN-PAGE standard (Fig. S4). We used α-DM as a detergent in this experiment, as it can solubilize
285 the grana core where the majority of the PSII-LHCII is localized. We observed the PSII-LHCII bands
286 (Fig. S4), which were not clearly shown in the lpCN-PAGE gel, using the digitonin-solubilized protein
287 complexes (Figs. 1, 3). It should be noted that α-DM could inhibit energy transfer from PSII to PSI within
288 the PSI-PSII megacomplex (Supplementary Fig. 14 in Yokono et al. 2015). Thus, digitonin is a better
289 detergent for the solubilization of the PSI-PSII megacomplex.
290 Then, we measured the fluorescence emission spectra of the PSI-LHCI, the PSII-LHCII, and
291 the LHCII trimer (Fig. S5). The identification of resolved bands was performed by silver-staining (Fig.
292 S6) and immunoblot analysis using the specific antibodies against PSI, PSII, LHCII, and LHCSR (Fig.
293 S7). The spectra of the *Physcomitrella* PSI–PSII megacomplex (Fig. 4) was found to be very similar to
294 those of the PSI–PSII megacomplex isolated from Arabidopsis (Yokono et al. 2015). A large fluorescence
295 peak at approximately 725 nm (Fig. 4) corresponded to low-energy chlorophylls in the PSI-LHCI (Fig.
296 S5). In addition, a much smaller broad peak at approximately 690 nm was observed. As the DM-
297 solubilized PSII-LHCII and LHCII trimer resolved by CN-PAGE showed fluorescence peaks at
298 approximately 693 nm and 678 nm (Fig. S5), the much smaller peak at approximately 690 nm might have
299 been emitted by PSII-LHCII (Fig. 4). These data suggested that the efficient energy transfer from PSII to
300 PSI occurred within the *Physcomitrella* PSI–PSII megacomplex, as observed in Arabidopsis (Yokono et
301 al. 2015). The small differences observed in the different fluorescence spectra before and after 1 h of

strong illumination (Fig. 4) implied that the strong illumination induced the *Physcomitrella* PSI–PSII megacomplex to transfer more excitation energy to low-energy chlorophylls in PSI, which may help *Physcomitrella* adapt to strong light conditions (Yokono et al. 2019).

Time-resolved fluorescence of the PSI–PSII megacomplex

To elucidate the fate of the excitation energy absorbed by the PSI–PSII megacomplex, we analyzed the fluorescence kinetics of the PSI–PSII megacomplex before and after 1 h of strong illumination (Fig. 5). The 1 h of illumination appeared to slightly increase the amounts of LHCSR and PsbS proteins (Fig. S8). In addition, 1 h of illumination strongly induced the conversion of violaxanthin to zeaxanthin (Table S1), which is required to achieve a high degree of NPQ in both the LHCSR– and PsbS–dependent pathways in *Physcomitrella* (Pinnola et al. 2013). It has previously been shown that PSII-LHCII supercomplexes with LHCSR have a greater quenching ability at low pH than that at neutral pH in *Chlamydomonas* (Tokutsu and Minagawa 2013). In addition, *Chlamydomonas* LHCSR1 is known to enhance energy transfer from LHCII to PSI at low pH (Kosuge et al. 2018). This implied that the *Physcomitrella* PSI–PSII megacomplex with LHCSR might show greater quenching ability at low pH. To test whether the PSI–PSII megacomplex with LHCSR showed a greater quenching ability at low pH, we measured the bands after soaking them in buffers that were adjusted to neutral pH (pH 7.0) or low pH (pH 4.5). The absorption

spectrum of the PSI–PSII megacomplexes was not significantly changed at low pH and under strong light illumination (Fig. S9).

The fluorescence decay-associated spectra of the PSI–PSII megacomplex isolated from the *Physcomitrella* cells without strong illumination are shown in Fig. 5a. Fluorescence lifetimes are summarized in Table S2. Under neutral pH conditions (Fig. 5a; solid lines), the kinetics were similar to those in the Arabidopsis megacomplex (Yokono et al. 2015). The first-lifetime component (~50 ps) reflects the fast energy migration between the PSII core antennae and the PSI core antennae. The fast energy migration between the PSII and the PSI core antennae strongly suggests that the binding between the PSII and the PSI was well-ordered, which also supports our hypothesis that the structure of *Physcomitrella* PSI–PSII megacomplex is similar to that of Arabidopsis megacomplex. In addition, the second to fifth components reflect trappings at the reaction centers and low-energy chlorophylls after energy migration. The sixth-lifetime component is the delayed fluorescence spectra, which reflects the excitation energy distribution after the direct excitation of the PSII reaction center. A larger peak originated from PSI-LHCI than that from PSII-LHCII in the sixth lifetime, which was suggestive of efficient energy transfer from PSII to PSI within the PSI–PSII megacomplex. The estimated spillover ratio did not show large changes under the different conditions (Table S2), suggesting that the balance of the energy distribution between the two photosystems was regulated without modification of the direct PSI–

PSII interaction. This behavior was also observed in the green algae *Chlamydomonas reinhardtii* and *Chlorella variabilis* (Ueno et al. 2018), but not in Arabidopsis (Yokono et al. 2015).

At a low pH, fast fluorescence decay was enhanced at approximately 710 nm (Fig. 5a, second-lifetime component). This tendency became more prominent under strong light growth conditions (Fig. 5b, second-lifetime component), indicating that the enhanced accumulation of zeaxanthin and/or the higher levels of the LHCSR and the PsbS induced fast fluorescence decay. The fluorescence at approximately 710 nm was thought to be emitted by an energy-dissipative state of LHCII and/or PSI (Iwai et al. 2010; Kosuge et al. 2018; Vasil'ev et al. 1997). The fast decrease in the fluorescence at approximately 710 nm (~200 ps) could be caused by quenching of the energy-dissipative state of LHCII or by the subsequent trapping at the PSI core (Bos et al. 2017; Mimuro et al. 2010). Conversely, the amplitude of the fluorescence at 740 nm, which reflects the trapping of the low-energy chlorophylls in LHCI (Iwai et al. 2015; Mazor et al. 2015) was decreased at low pH (Fig. 5, fifth-lifetime component). This also implies that the energy was dissipated around LHCII and/or was trapped in the PSI core before it reached LHCI. The enhanced 710 nm peak was also observed in the delayed fluorescence spectra (Fig. 5, sixth-lifetime component), reflecting the diversification of the destination of the energy transfer from PSII.

Discussion

Isolation of the PSI–PSII megacomplex with LHCSR in *Physcomitrella* by lpCN-PAGE

In the present study, the PSI–PSII megacomplex in the protonemata of *Physcomitrella* was resolved by the lpCN-PAGE (Figs. 1, 3). The movement of the *Physcomitrella* PSI–PSII megacomplex band through the sample gel showed that the band was not partially solubilized membrane particles, but a huge protein complex (<10 MDa) (Strecker et al. 2010). The similar migration distance of the *Physcomitrella* PSI–PSII megacomplex to the Arabidopsis megacomplex in lpCN-PAGE (Fig. 3) showed that these complexes are similar in size (Yokono et al. 2019). We recently proposed the first structural model of the Arabidopsis PSI–PSII megacomplex that consists of one PSII dimer sandwiched between two PSI-LHCI complexes with the additional LHCII trimers surrounded peripherally, based on the negatively stained EM particles (Yokono et al. 2019). The similarities in molecular size, the 77K steady-state fluorescence spectra (Fig. 4), and the fluorescence kinetics (Fig. 5) of the *Physcomitrella* PSI–PSII megacomplex to the Arabidopsis megacomplex strongly suggest that the molecular structures of the *Physcomitrella* PSI–PSII and Arabidopsis megacomplexes are similar (Yokono et al. 2019). However, further studies will be required to confirm this.

In addition, fast energy transfer occurred from the PSII to PSI cores in the *Physcomitrella* PSI–PSII megacomplex (Fig. 5, first-lifetime component), which suggests a direct interaction between the PSII and PSI cores (Yokono and Akimoto 2018; Yokono et al. 2015). It should be noted that only the co-migration of the PSII and the PSI did not show energy transfer between them as seen in our previous data

(w2 and w3 bands shown in Fig. 1c in Yokono et al. 2015), suggesting that a well-ordered assembly of the PSI–PSII megacomplex is essential for achieving a rapid energy transfer from PSII to PSI (Fig. 5).

In addition to the PSI, PSII, and LHCs that are also found in the Arabidopsis PSI–PSII megacomplexes, the *Physcomitrella* PSI–PSII megacomplex contained LHCSR, which plays an important role in the protection of photosystems by dissipating excess energy in *Chlamydomonas* (Peers et al. 2009) and *Physcomitrella* (Alboresi et al. 2010). The co-migration of PSII-LHCII with LHCSR was also observed by CN-PAGE (Fig. S7), suggesting that LHCSR associates not only with the PSI-PSII megacomplex but also with the PSII-LHCII megacomplex in *Physcomitrella* (Fig. S7). Furthermore, we also found the presence of PsbS in the *Physcomitrella* PSI-PSII megacomplex (Fig. S3). This finding is consistent with a previous report that PsbS is included in the Arabidopsis PSI-PSII megacomplex (Suorsa et al. 2015). The presence of LHCSR and PsbS in the *Physcomitrella* PSI–PSII megacomplex implies that heat dissipation of the excitation energy absorbed by them plays an important role in mitigating photo-oxidative damage in the megacomplex.

pH-dependent quenching in the PSI–PSII megacomplex

At low pH conditions, fast trapping (~200 ps) at approximately 710 nm was enhanced and, concomitantly, trapping at low-energy chlorophylls in LHCI (740 nm) was suppressed (Fig. 5). We assumed that the fast decay in the chlorophyll fluorescence at approximately 710 nm originated from the energy-dissipative

state of LHCII and/or by subsequent trapping at the PSI core. The energy transfer rate from the PSII core to the PSI core was not altered, even at low pH (first lifetime component (~50 ps) in Fig. 5). This implied that the enhancement of fast trapping at approximately 710 nm was not responsible for the change in the PSI core itself in response to the low pH conditions but was responsible for the change in the peripheral LHCII in the PSI–PSII megacomplex of *Physcomitrella*. It should be noted that the existence of an energy transfer pathway from LHCII to PSI that does not involve LHCI has already been reported (Benson et al. 2015; Ferroni et al. 2018). If an additional quenching site is activated in the peripheral LHCII at a low pH, it will accept energy from the PSI core.

A recent study suggested that LHCSR might bind to LHCII in PSI-LHCI/II in *Physcomitrella* (Pinnola et al. 2015) and that LHCSR mediates pH-dependent quenching (Pinnola et al. 2017; Tokutsu and Minagawa 2013). Pinnola et al. (2015) suggested that LHCSR does not directly quench PSI-LHCI, but instead quench it by modulating the lifetime of an LHCII population (Pinnola et al. 2015, 2017). Moreover, *Chlamydomonas* cells that possessed both LHCII and LHCSR exhibited a 710-nm fluorescence maximum at 77 K and displayed pH-dependent quenching (Dinc et al. 2016). Combined with these data, we suggested that LHCSR binds to peripheral LHCII in the *Physcomitrella* PSI–PSII megacomplex and quenches the excitation energy via a pH- or zeaxanthin-dependent manner.

In addition to LHCSR, previous studies showed that PsbS also binds to LHCII in the PSII-LHCII and contributes to forming NPQ in both a pH- and a zeaxanthin-dependent manner (Correa-Galvis

et al. 2016; Sacharz et al. 2017). Thus, it is possible to speculate that both LHCSR and PsbS can contribute the pH-dependent quenching in the *Physcomitrella* megacomplex.

P. patens utilization of shallower low-energy chlorophylls

Plants possess various low-energy chlorophylls in the PSI-LHCI. In the fluorescence decay-associated spectrum of the *Physcomitrella* PSI–PSII megacomplex (Fig. 5), fluorescence at 710 nm, 720 nm, 730 nm, and 740 nm was detected in the second to fifth-lifetime components (summarized in Table 1), respectively. Meanwhile, the Arabidopsis PSI–PSII megacomplex showed fluorescence peaks at 720 nm, 725 nm, 735 nm, and 740 nm (Fig. S3b in Yokono et al. (2015)). The difference in the composition of the low-energy chlorophylls between Arabidopsis and *Physcomitrella* might reflect the variations in the LHCI proteins in *Physcomitrella* (Busch et al. 2013).

From a functional perspective, low-energy chlorophylls are classified into two types, shallower and deeper low-energy chlorophylls, depending on their energy levels. In the green lineage, the PSI core possesses shallower low-energy chlorophylls, whereas LHCI possesses deeper low-energy chlorophylls (Kunugi et al. 2016). Typically, shallower low-energy chlorophylls show fluorescence maxima at approximately 720 nm or shorter and possess a large Förster overlap integral at P700. They can transfer excitation energy to P700 via the uphill energy transfer process (Melkozernov and Blankenship 2005; Melkozernov et al. 2004). Conversely, deeper low-energy chlorophylls in PSI-LHCI can dissipate

excitation energy as heat by the following two mechanisms (reviewed by Yokono and Akimoto 2018). The first mechanism depends on their ability to transfer excitation energy to $P700^+$ (Schlodder et al. 2011; Shubin et al. 1995). Their fluorescence maxima of approximately 725 nm or longer enables them to possess a large Förster overlap integral at $P700^+$. Since $P700^+$ is an excellent quencher (Croce and van Amerongen 2013), their ability to transfer energy to $P700^+$ should contribute to the dissipation of excess energy as heat.

The second mechanism depends on their ability to form a charge-transfer state with a carotenoid, which also enables them to dissipate excess energy as heat (Ballottari et al. 2014). Owing to these two mechanisms, PSI-LHCI tends to tolerate high levels of illumination as it has deeper low-energy chlorophylls (Yokono et al. 2019). Both *Physcomitrella* and Arabidopsis possess shallower and deeper low-energy chlorophylls. In the *Physcomitrella* PSI–PSII megacomplex, 72% of the amplitude was occupied by the shallower low-energy chlorophylls, whereas in the Arabidopsis PSI–PSII megacomplex, 72% of the amplitude was occupied by the deeper low-energy chlorophylls (Table 1). The amplitude reflects the probability of energy acceptance of each low-energy chlorophyll. Therefore, the excitation energy absorbed by *Physcomitrella* PSI–PSII was mainly transferred to P700 to perform photosynthesis, and the heat-dissipation processes may show lower efficiency depending on the deeper low-energy chlorophylls. In contrast, the excitation energy absorbed by Arabidopsis PSI–PSII was primarily dissipated as heat rather than being utilized for photosynthesis. The difference between *Physcomitrella*

444 and Arabidopsis might be related to the structural differences in PSI-LHCI. Arabidopsis PSI-LHCI
445 possesses one layer of the LHCI belt containing four Lhca proteins, which are all in the range of the
446 Förster critical distance from $P700^+$ (< 80–90Å) (Mazor et al. 2015; van Grondelle 1985). Therefore, all
447 the deeper low-energy chlorophylls in the LHCI belt in Arabidopsis might participate in the energy
448 transfer to $P700^+$ to dissipate the excitation energy (Yokono and Akimoto 2018). Conversely,
449 *Physcomitrella* possesses two layers of the LHCI belt containing eight Lhca proteins (Iwai et al. 2018),
450 although the second layer may be beyond the range of the Förster critical distance. Thus, even if the
451 second layer of the LHCI belt possesses the deeper low-energy chlorophylls, they may not efficiently
452 perform $P700^+$-dependent quenching. Alternatively, *Physcomitrella* possesses LHCSR and PsbS that
453 could bind to the peripheral LHCII around PSI-LHCI (Pinnola et al. 2015, 2017) and PSII-LHCII
454 (Correa-Galvis et al. 2016; Sacharz et al. 2017) and act as a quencher that possibly works with shallower
455 low-energy chlorophylls.
456
457 **Possible photoprotection strategy in *P. patens***
458 In *Physcomitrella*, the shallower low-energy chlorophylls can efficiently transfer absorbed energy to P700
459 to perform photosynthesis (Yokono and Akimoto 2018). When the light becomes strong, *Physcomitrella*
460 induces the accumulation of PsbS and LHCSR proteins (Gerotto et al. 2011). Recent studies have shown
461 that *Chlamydomonas* LHCSR proteins are induced by blue light (Petroutsos et al. 2016) and UV (Allorent

et al. 2016; Tilbrook et al. 2016; Tokutsu et al. 2019). If mosses possess similar mechanisms to induce LHCSR proteins in response to blue light and UV, this should contribute to their adaptation to terrestrial environments. However, PsbS localizes in the grana stack and can dissipate the excitation energy that is absorbed by PSII-LHCII as heat (Pinnola et al. 2015). Thus, under high levels of illumination, linear electron transfer is suppressed by the PsbS-dependent NPQ and can be reduced in favor of cyclic electron flow (Allahverdiyeva et al. 2015). $P700^+$ may accumulate within the PSI–PSII megacomplex in the grana margin and excitation energy trapped by the deeper low-energy chlorophylls in the PSI–PSII megacomplex is efficiently dissipated by $P700^+$. This scenario is likely occurring in Arabidopsis (Fig. 6). However, the energy transfer capacity of the deeper low-energy chlorophylls was limited in *Physcomitrella* (Fig. 5, Table S2). Instead, LHCSR can dissipate the excitation energy trapped by PSI (Pinnola et al. 2015), which may help survive in strong light conditions. The 710 nm chlorophylls in the putative peripheral LHCII of the *Physcomitrella* PSI–PSII megacomplex might shift the energy distribution toward the quenching site, which may enhance energy dissipation efficiency under low pH conditions (Yokono et al. 2018). This hypothetical scheme should work well under high light conditions (Fig. 6), although further studies are required to verify this hypothesis.

One limitation of this study is that no information was obtained on how changes in the PSI–PSII megacomplex related to the developmental stages of *Physcomitrella*. Future studies, including the

479 comparison of the PSI–PSII megacomplex in the protonemata and gametophore, will be important for
480 understanding the function of PSI–PSII megacomplex in the developmental of *Physcomitrella*.
481
482 **Conclusion**
483 In this study, we isolated a *Physcomitrella* PSI–PSII megacomplex, which is also present in Arabidopsis
484 *thaliana* (Yokono et al. 2015), *Selaginella martensii* (Ferroni et al. 2016), and *Neochloris oleoabundans*
485 (Giovanardi et al. 2017). The presence of the PSI–PSII megacomplex in these green plants suggests that
486 the PSI–PSII megacomplex is widely prevalent among land plants. However, the presence of LHCSR in
487 the *Physcomitrella* PSI–PSII megacomplex is unique and does not occur in Arabidopsis. Given the
488 molecular and physiological function of LHCSR, the LHCSR, together with PsbS in the megacomplex
489 might assist in dissipating excess light energy as heat. We also observed that the chlorophyll fluorescence
490 spectra with a peak of 710 nm were enhanced under low pH conditions—something that was not
491 observed in the Arabidopsis PSI–PSII megacomplex. This observation can be explained by assuming that
492 LHCSR and/or PsbS bind at the additional LHCII that was not present in the Arabidopsis PSI–PSII
493 megacomplex and enhances heat dissipation under the high light illumination.
494 In conclusion, our results from this study provide new insights into the regulation of
495 photosynthesis in response to light conditions in *Physcomitrella*.
496

497 **References**

498 Alboresi A, Gerotto C, Giacometti GM, Bassi R, Morosinotto T (2010) *Physcomitrella patens* mutants
499 affected on heat dissipation clarify the evolution of photoprotection mechanisms upon land colonization.
500 Proc Natl Acad Sci USA 107:11128-11133. https://doi:10.1073/pnas.1002873107

501

502 Allahverdiyeva Y, Suorsa M, Tikkanen M, Aro EM (2015) Photoprotection of photosystems in fluctuating
503 light intensities. J Exp Bot 66:2427-2436. https://doi:10.1093/jxb/eru463

504

505 Allorent G, Lefebvre-Legendre L, Chappuis R, Kuntz M, Truong TB, Niyogi KK, Ulm R, Goldschmidt-
506 Clermont M (2016) UV-B photoreceptor-mediated protection of the photosynthetic machinery in
507 *Chlamydomonas reinhardtii*. Proc Natl Acad Sci USA 20;113:14864-14869. https;//doi:
508 10.1073/pnas.1607695114.

509

510 Ballottari M, Alcocer MJ, D'Andrea C, Viola D, Ahn TK, Petrozza A, Polli D, Fleming GR, Cerullo G,
511 Bassi R (2014) Regulation of photosystem I light-harvesting by zeaxanthin. Proc Natl Acad Sci USA 111:
512 E2431-2438. https://doi:10.1073/pnas.1404377111

513

514 Benson SL, Maheswaran P, Ware MA, Hunter CN, Horton P, Jansson S, Ruban AV, Johnson MP (2015)
515 An intact light-harvesting complex I antenna system is required for complete state transitions in
516 Arabidopsis. Nature Plant 1:15176. https://doi:10.1038/nplants.2015.176
517
518 Bellafiore S, Barneche F, Peltier G, Rochaix JD (2005) State transitions and light adaptation require
519 chloroplast thylakoid protein kinase STN7. Nature 433:892-5. https://doi.org/10.1038/nature03286
520 Bos I, Bland KM, Tian LJ, Croce R, Frankel LK, van Amerongen H, Bricker TM, Wientjes E (2017)
521 Multiple LHCII antennae can transfer energy efficiently to a single Photosystem I. Biochim Biophys Acta
522 1858:371-378. https://doi:10.1016/j.bbabio.2017.02.012
523
524 Bonente G, Ballottari M, Truong TB, Morosinotto T, Ahn TK, Fleming GR, Niyogi KK, Bassi R (2011)
525 Analysis of LhcSR3, a protein essential for feedback de-excitation in the green alga *Chlamydomonas*
526 *reinhardtii.* PLOS Biol. 9:e1000577. https://doi: 10.1371/journal.pbio.1000577.
527
528 Busch A, Petersen J, Webber-Birungi MT, Powikrowska M, Lassen LM, Naumann-Busch B, Nielsen AZ,
529 Ye J, Boekema EJ, Jensen ON, Lunde C, Jensen PE (2013) Composition and structure of photosystem I in
530 the moss *Physcomitrella patens*. J Exp Bot 64:2689-2699. https://doi:10.1093/jxb/ert126
531

532 Correa-Galvis V, Poschmann G, Melzer M, Stühler K, Jahns P (2016) PsbS interactions involved in the
533 activation of energy dissipation in *Arabidopsis*. Nat Plants 2:15225. https://doi:10.1038/nplants.2015.225.
534
535 Correa-Galvis V, Redekop P, Guan K, Griess A, Truong TB, Wakao S, Niyogi KK, Jahns P (2016)
536 Photosystem II subunit PsbS is involved in the induction of LHCSR protein-dependent energy dissipation
537 in *Chlamydomonas reinhardtii*. J Biol Chem 291:17478-17487. https://doi:10.1074/jbc.M116.737312
538
539 Croce R, van Amerongen H (2013) Light-harvesting in photosystem I. Photosynth Res 116:153-166.
540 https://doi:10.1007/s11120-013-9838-x
541
542 Dinc E, Tian L, Roy LM, Roth R, Goodenough U, Croce R (2016) LHCSR1 induces a fast and reversible
543 pH-dependent fluorescence quenching in LHCII in *Chlamydomonas reinhardtii* cells. Proc Natl Acad Sci
544 USA 113 (27):7673-7678. https://doi:10.1073/pnas.1605380113
545
546 Ferroni L, Suorsa M, Aro EM, Baldisserotto C, Pancaldi S (2016) Light acclimation in the lycophyte
547 *Selaginella martensii* depends on changes in the number of photosystems and on the flexibility of the
548 light-harvesting complex II antenna association with both photosystems. New Phytol 211:554-568.
549 https://doi:10.1111/nph.13939

Ferroni L, Cucuzza S, Angeleri M, Aro EM, Pagliano C, Giovanardi M, Baldisserotto C, Pancaldi S (2018) In the lycophyte *Selaginella martensii* is the "extra-qT" related to energy spillover? Insights into photoprotection in ancestral vascular plants. Enrion Exp Bot 154:110-122. https://doi.org/10.1016/j.envexpbot.2017.10.023

Giovanardi M, Poggioli M, Ferroni L, Lespinasse M, Baldisserotto C, Aro EM, Pancaldi S (2017) Higher packing of thylakoid complexes ensures a preserved Photosystem II activity in mixotrophic *Neochloris oleoabundans*. Algal Res 25:322-332. https://doi.org/10.1016/j.algal.2017.05.020

Gerotto C, Alboresi A, Giacometti GM, Bassi R, Morosinotto T (2011) Role of PSBS and LHCSR in *Physcomitrella patens* acclimation to high light and low temperature. Plant Cell Environ 34:922-932. https://doi:10.1111/j.1365-3040.2011.02294.x

Goss R, Lepetit B (2015) Biodiversity of NPQ. J Plant Physiol 172:13-32. https://doi:10.1016/j.jplph.2014.03.004

567 Iwai M, Yokono M (2017) Light-harvesting antenna complexes in the moss *Physcomitrella patens*:
568 implications for the evolutionary transition from green algae to land plants. Curr Opin Plant Biol 37:94-
569 101. https://doi:10.1016/j.pbi.2017.04.002
570
571 Iwai M, Yokono M, Inada N, Minagawa J (2010) Live-cell imaging of photosystem II antenna
572 dissociation during state transitions. Proc Natl Acad Sci U S A 107:2337-2342.
573 https://doi:10.1073/pnas.0908808107
574
575 Iwai M, Yokono M, Kono M, Noguchi K, Akimoto S, Nakano A (2015) Light-harvesting complex Lhcb9
576 confers a green alga-type photosystem I supercomplex to the moss *Physcomitrella patens*. Nature Plants
577 1:14008. https://doi:10.1038/nplants.2014.8
578 Iwai M, Grob P, Iavarone AT, Nogales E, Niyogi KK (2018) A unique supramolecular organization of
579 photosystem I in the moss *Physcomitrella patens*. Nature Plants 4:904-909. https;//doi: 10.1038/s41477-
580 018-0271-1.
581
582 Järvi S, Suorsa M, Paakkarinen V, Aro EM (2011) Optimized native gel systems for separation of
583 thylakoid protein complexes: novel super- and mega-complexes. Biochem J 439:207-214.
584 https://doi:10.1042/BJ20102155

585

586 Kondo T, Pinnola A, Chen WJ, Dall'Osto L, Bassi R, Schlau-Cohen GS (2017) Single-molecule

587 spectroscopy of LHCSR1 protein dynamics identifies two distinct states responsible for multi-timescale

588 photosynthetic photoprotection. Nature Chem 9:772-778. https://doi: 10.1038/nchem.2818.

589

590 Kosuge K, Tokutsu R, Kim E, Akimoto S, Yokono M, Ueno Y, Minagawa J (2018) LHCSR1-dependent

591 fluorescence quenching is mediated by excitation energy transfer from LHCII to photosystem I in

592 *Chlamydomonas reinhardtii*. Proc Natl Acad Sci U S A 115:3722-3727.

593 https://doi:10.1073/pnas.1720574115

594

595 Kunugi M, Satoh S, Ihara K, Shibata K, Yamagishi Y, Kogame K, Obokata J, Takabayashi A, Tanaka A

596 (2016) Evolution of green plants accompanied changes in light-harvesting systems. Plant Cell Physiol

597 57:1231-1243. https:// doi:10.1093/pcp/pcw071

598

599 Mazor Y, Borovikova A, Nelson N (2015) The structure of plant photosystem I super-complex at 2.8 A

600 resolution. Elife 4:e07433. https://doi:10.7554/eLife.07433

601

602 Melkozernov AN, Blankenship RE (2005) Structural and functional organization of the peripheral light-
603 harvesting system in photosystem I. Photosynth Res 85:33-50. https://doi:10.1007/s11120-004-6474-5
604
605 Melkozernov AN, Kargul J, Lin S, Barber J, Blankenship RE (2004) Energy coupling in the PSI-LHCI
606 supercomplex from the green alga *Chlamydomonas reinhardtii*. J Phys Chem B 108:10547-10555.
607 https://doi:10.1021/jp049375n
608
609 Mimuro M, Yokono M, Akimoto S (2010) Variations in photosystem I properties in the primordial
610 cyanobacterium *Gloeobacter violaceus* PCC 7421. Photochem Photobiol 86:62-69.
611 https://doi:10.1111/j.1751-1097.2009.00619.x
612
613 Minagawa J, Tokutsu R (2015) Dynamic regulation of photosynthesis in *Chlamydomonas reinhardtii*.
614 Plant J 82:413-428. https://doi:10.1111/tpj.12805
615
616 Nishiyama T, Hiwatashi Y, Sakakibara I, Kato M, Hasebe M (2000) Tagged mutagenesis and gene-trap in
617 the moss, *Physcomitrella patens* by shuttle mutagenesis. DNA Res 7:9-17.
618 https://doi:10.1093/dnares/7.1.9
619

620 Niyogi KK, Truong TB (2013) Evolution of flexible non-photochemical quenching mechanisms that
621 regulate light harvesting in oxygenic photosynthesis. Curr Opin Plant Biol 16:307-314.
622 https://doi:10.1016/j.pbi.2013.03.011
623
624 Peers G, Truong TB, Ostendorf E, Busch A, Elrad D, Grossman AR, Hippler M, Niyogi KK (2009) An
625 ancient light-harvesting protein is critical for the regulation of algal photosynthesis. Nature 462:518-521.
626 https://doi:10.1038/nature08587
627
628 Pesaresi P, Hertle A, Pribil M, Kleine T, Wagner R, Strissel H, Ihnatowicz A, Bonardi V, Scharfenberg M,
629 Schneider A, Pfannschmidt T, Leister D (2009) Arabidopsis STN7 kinase provides a link between short-
630 and long-term photosynthetic acclimation. Plant Cell 21:2402-23. https://doi:10.1105/tpc.108.064964.
631
632 Petroutsos D, Tokutsu R, Maruyama S, Flori S, Greiner A, Magneschi L, Cusant L, Kottke T, Mittag M,
633 Hegemann P, Finazzi G, Minagawa J (2016) A blue-light photoreceptor mediates the feedback regulation
634 of photosynthesis. Nature 537:563-566. https://doi:10.1038/nature19358
635

636 Pinnola A, Ballottari M, Bargigia I, Alcocer M, D'Andrea C, Cerullo G, Bassi R (2017) Functional
637 modulation of LHCSR1 protein from *Physcomitrella patens* by zeaxanthin binding and low pH. Sci Rep
638 7:11158. https://doi:10.1038/s41598-017-11101-7
639
640 Pinnola A, Cazzaniga S, Alboresi A, Nevo R, Levin-Zaidman S, Reich Z, Bassi R (2015) Light-harvesting
641 complex stress-related proteins catalyze excess energy dissipation in both photosystems of *Physcomitrella*
642 *patens*. Plant Cell 27:3213-3227. https://doi:10.1105/tpc.15.00443
643
644 Pinnola A, Dall'Osto L, Gerotto C, Morosinotto T, Bassi R, Alboresi A. (2013) Zeaxanthin binds to light-
645 harvesting complex stress-related protein to enhance nonphotochemical quenching in *Physcomitrella*
646 *patens*. Plant Cell 25:3519-34. https://doi: 10.1105/tpc.113.114538.
647
648 Popot JL, Althoff T, Bagnard D, Baneres JL, Bazzacco P, Billon-Denis E, Catoire LJ, Champeil P,
649 Charvolin D, Cocco MJ, Cremel G, Dahmane T, de la Maza LM, Ebel C, Gabel F, Giusti F, Gohon Y,
650 Goormaghtigh E, Guittet E, Kleinschmidt JH, Kuhlbrandt W, Le Bon C, Martinez KL, Picard M, Pucci B,
651 Sachs JN, Tribet C, van Heijenoort C, Wien F, Zito F, Zoonens M (2011) Amphipols from A to Z. Annu
652 Rev Biophys 40:379-408. https://doi:10.1146/annurev-biophys-042910-155219
653

654 Rantala M, Tikkanen M, Aro EM (2017) Proteomic characterization of hierarchical megacomplex
655 formation in Arabidopsis thylakoid membrane. Plant J 92:951-962. https://doi:10.1111/tpj.13732
656
657 Ruban AV (2015) Evolution under the sun: optimizing light harvesting in photosynthesis. J Exp Bot 66:7-
658 23. https://doi:10.1093/jxb/eru400
659
660 Ruban AV (2016) Nonphotochemical chlorophyll fluorescence quenching: mechanism and effectiveness
661 in protecting plants from photodamage. Plant Physiol 170:1903-1916. https://doi:10.1104/pp.15.01935
662
663 Sacharz J, Giovagnetti V, Ungerer P, Mastroianni G, Ruban AV (2017) The xanthophyll cycle affects
664 reversible interactions between PsbS and light-harvesting complex II to control non-photochemical
665 quenching. Nature Plants 3:16225. https://doi: 10.1038/nplants.2016.225.
666
667 Schlodder E, Hussels M, Çetin M, Karapetyan NV, Brecht M (2011) Fluorescence of the various red
668 antenna states in photosystem I complexes from cyanobacteria is affected differently by the redox state of
669 P700. Biochim Biophys Acta 1807: 1423–1431. https://doi:10.1016/j.bbabio.2011.06.018
670

671 Shubin VV, Bezsmertnaya IN, Karapetyan NV (1995) Efficient energy-transfer from the long-wavelength
672 antenna chlorophylls to P700 in photosystem-I complexes from *Spirulina platensis*. J Photoch Photobio B
673 30:153-160. https://doi:10.1016/1011-1344(95)07173-Y
674
675 Strecker V, Wumaier Z, Wittig I, Schägger H (2010) Large pore gels to separate mega protein complexes
676 larger than 10 MDa by blue native electrophoresis: isolation of putative respiratory strings or patches.
677 Proteomics 10:3379-87. https://doi:10.1002/pmic.201000343
678
679 Suorsa M, Rantala M, Danielsson R, Jarvi S, Paakkarinen V, Schroder WP, Styring S, Mamedov F, Aro
680 EM (2014) Dark-adapted spinach thylakoid protein heterogeneity offers insights into the photosystem II
681 repair cycle. Biochim Biophys Acta 1837:1463-1471. https://doi:10.1016/j.bbabio.2013.11.014
682
683 Suorsa M, Rantala M, Mamedov F, Lespinasse M, Trotta A, Grieco M, Vuorio E, Tikkanen M, Jarvi S,
684 Aro EM (2015) Light acclimation involves dynamic re-organization of the pigment-protein
685 megacomplexes in non-appressed thylakoid domains. Plant J 84:360-373. https://doi:10.1111/tpj.13004
686

687 Tilbrook K, Dubois M, Crocco CD, Yin R, Chappuis R, Allorent G, Schmid-Siegert E, Goldschmidt-
688 Clermont M, Ulm R (2016) UV-B Perception and Acclimation in *Chlamydomonas reinhardtii*. Plant Cell
689 28:966-83. https://doi: 10.1105/tpc.15.00287.
690
691 Tokutsu R, Minagawa J (2013) Energy-dissipative supercomplex of photosystem II associated with
692 LHCSR3 in *Chlamydomonas reinhardtii*. Proc Natl Acad Sci U S A 110:10016-10021.
693 https://doi:10.1073/pnas.1222606110
694
695 Tokutsu R, Fujimura-Kamada K, Yamasaki T, Matsuo T, Minagawa J (2019) Isolation of photoprotective
696 signal transduction mutants by systematic bioluminescence screening in *Chlamydomonas reinhardtii*. Sci
697 Rep 26;9:2820. https;//doi: 10.1038/s41598-019-39785-z.
698
699 Ueno Y, Aikawa S, Kondo A, Akimoto S (2018) Adaptation of light-harvesting functions of unicellular
700 green algae to different light qualities. Photosynth Res 139:145-154. https://doi:10.1007/s11120-018-
701 0523-y
702

703 Umetani I, Kunugi M, Yokono M, Takabayashi A, Tanaka A (2018) Evidence of the supercomplex
704 organization of photosystem II and light-harvesting complexes in *Nannochloropsis granulata*. Photosynth
705 Res 136:49-61. https://doi:10.1007/s11120-017-0438-z
706
707 Van Grondelle R (1985) Excitation-energy transfer, trapping and annihilation in photosynthetic systems.
708 Biochim Biophys Acta 811:147-195. https://doi:10.1016/0304-4173(85)90017-5
709
710 Vasil'ev S, Irrgang KD, Schrotter T, Bergmann A, Eichler HJ, Renger G (1997) Quenching of chlorophyll
711 a fluorescence in the aggregates of LHCII: steady-state fluorescence and picosecond relaxation kinetics.
712 Biochemistry 36:7503-7512. https://doi:10.1021/bi9625253
713
714 Watanabe A, Kim E, Burton-Smith RN, Tokutsu R, Minagawa J (2019) Amphipol-assisted purification
715 method for the highly active and stable photosystem II supercomplex of *Chlamydomonas reinhardtii*.
716 FEBS Lett 593:1072-1079. https://doi:10.1002/1873-3468.13394
717
718 Wobbe L, Bassi R, Kruse O (2016) Multi-level light capture control in plants and green algae. Trends
719 Plant Sci 21:55-68. https://doi:10.1016/j.tplants.2015.10.004
720

721 Xu DQ, Chen Y, Chen GY (2015) Light-harvesting regulation from leaf to molecule with the emphasis on
722 rapid changes in antenna size. Photosynth Res 124:137-158. https://doi:10.1007/s11120-015-0115-z
723
724 Yokono M, Akimoto S (2018) Energy transfer and distribution in photosystem super/megacomplexes of
725 plants. Curr Opin Biotechnol 54:50-56. https://doi:10.1016/j.copbio.2018.01.001
726
727 Yokono M, Takabayashi A, Akimoto S, Tanaka A (2015) A megacomplex composed of both photosystem
728 reaction centres in higher plants. Nat Commun 6. https://doi:10.1038/ncomms7675
729
730 Yokono M, Umetani I, Takabayashi A, Akimoto S, Tanaka A (2018) Regulation of excitation energy in
731 *Nannochloropsis* photosystem II. Photosynth Res 139:155-161. https://doi:10.1007/s11120-018-0510-3
732
733 Yokono M, Takabayashi A, Kishimoto J, Fujita T, Iwai M, Murakami A, Akimoto S, Tanaka A (2019) The
734 PSI-PSII megacomplex in green plants. Plant Cell Phyiol accepted. https://doi.org/10.1093/pcp/pcz026
735
736 **Figure legends**
737 **Fig. 1** Separation of thylakoid pigment-protein complexes in *Physcomitrella* by lpCN-PAGE with
738 Amphipol A8-35. The thylakoid membrane proteins from the protonemata cells grown under low-light

739 (40 µmol photons m^{-2} s^{-1}) conditions and the cells illuminated under strong light (500 µmol photons m^{-2}

740 s^{-1}) for 1 h were solubilized with 1% digitonin and were separated by 3.5%–13% polyacrylamide.

741

742 **Fig. 2** Immunoblot analyses of PsbB (PSII), PsbC (PSII), PsaB (PSI), Lhcb2 (LHCII), Lhcb3 (LHCII),

743 and LHCSR proteins after 2D-lpCN/SDS-PAGE of the thylakoid protein complexes in *Physcomitrella*

744 protonemata grown under low-light conditions.

745

746 **Fig. 3** Separation of the Arabidopsis and *Physcomitrella* thylakoid protein complexes by lpCN-PAGE

747 using gels of different acrylamide concentrations (a: 3%–13%; b: 3.25%–13%). Thylakoid protein

748 complexes were solubilized in 1% digitonin. The sample gel (C20) was made by using an acrylamide

749 solution of 3% T and 20% C (Strecker et al. 2010).

750

751 **Fig. 4** Steady-state fluorescence spectra of the PSI–PSII megacomplex (Fig. 1). The measurement

752 temperature was 77 K. The upper graph shows the spectrum isolated from thalli grown under low-light

753 conditions; the middle graph shows the spectrum isolated from thalli grown under high light conditions;

754 while the lower graph shows the difference spectrum between the cells grown under low-light-conditions

755 and those illuminated under a strong light.

756

757 **Fig. 5** Fluorescence decay-associated spectra of PSI–PSII megacomplex isolated from a) low light-grown
758 cell and b) high light grown cell. Solid line (pH 7), dotted line (pH 4.5). Measurement temperature was 77
759 K. Lifetimes are summarized in Table S2.
760
761 **Fig. 6** Schematic model of the PSI–PSII megacomplex in Arabidopsis and *Physcomitrella*. The large and
762 small circles represent the LHCII trimer and monomer, respectively. If the energy was trapped by the
763 deeper low-energy chlorophylls (Chls), it could be dissipated efficiently. However, if the energy was
764 trapped by the shallower low-energy Chls, uphill energy transfer occurred to P700 under physiological
765 temperatures, and the energy could then be utilized for photosynthesis. In Arabidopsis, the PSI core has
766 shallower low-energy Chls, whereas the LHCI belt has deeper low-energy Chls. Digitonin-sensitive
767 LHCII could transfer energy to the PSI core via LHCI (Benson et al. 2015). In contrast, the PSI in
768 *Physcomitrella* has a second LHCI belt, which was not found in Arabidopsis, in addition to the first LHCI
769 belt. Shallower low-energy Chls may exist in the additional LHCII of the *Physcomitrella* PSI–PSII
770 megacomplex, which might transfer energy directly to the PSI core. Differences in the LHCII binding
771 sites may affect the course of the excitation energy. Under strong light conditions, LHCSR in the
772 *Physcomitrella* PSI–PSII megacomplex probably dissipates the excitation energy.
773
774

775

776

777

778

779

780

781

782

783

784

785

786

787

788

789 **Tables**

790 Table 1. The amplitude ratio of low-energy chlorophylls

Physcomitrella patens

Peak wavelength	Lifetime	Amplitude	Amplitude ratio (%)	deeper ratio (%)
710 nm	200 ps	1.5	36	28
720 nm	750 ps	1.5	36	
730 nm	1.9 ns	1.1	26	
740 nm	4.1 ns	0.08	2	

Arabidopsis thaliana (from Yokono et al. (2015))

Peak wavelength	Lifetime	Amplitude	Amplitude ratio (%)	deeper ratio (%)
720 nm	240 ps	0.35	28	72
725 nm	1.0 ns	0.26	20	
735 nm	2.2 ns	0.44	35	
740 nm	3.3 ns	0.22	17	

791

Fig. 1

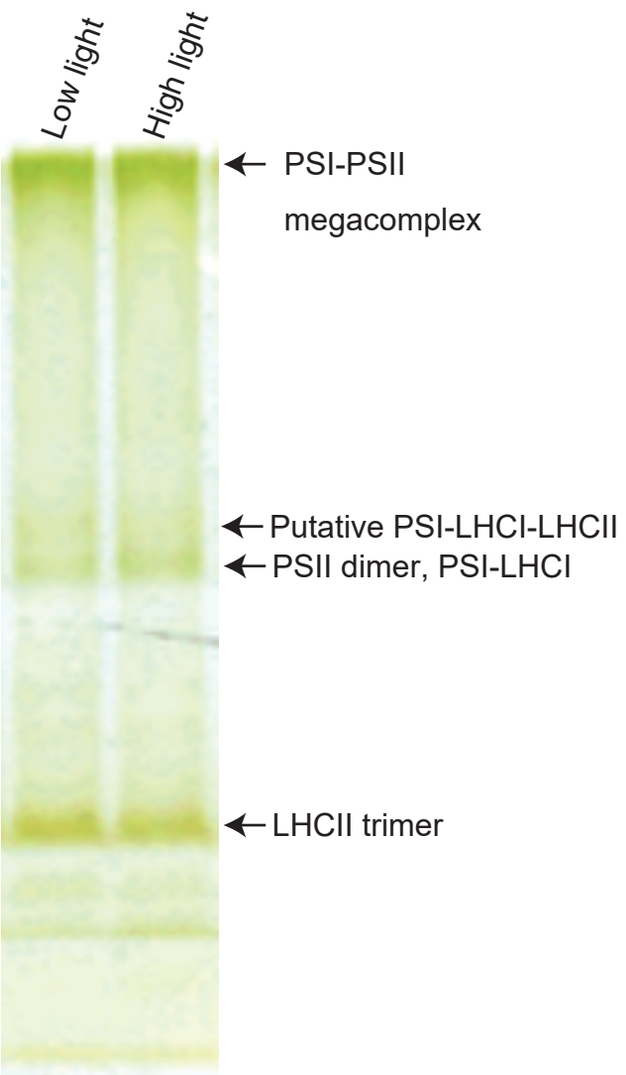

Furukawa et al.

Fig. 2

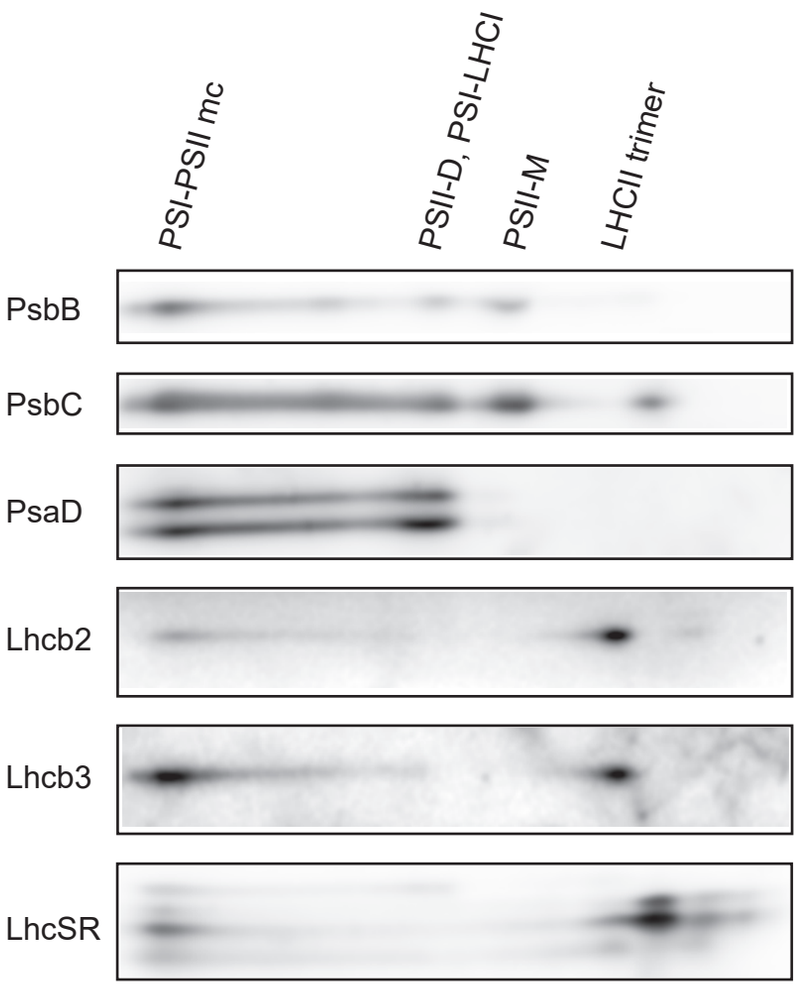
PSI-PSII mc
PSII-D, PSI-LHCI
PSII-M
LHCII trimer
PsbB
PsbC
PsaD
Lhcb2
Lhcb3
LhcSR

Fig. 3

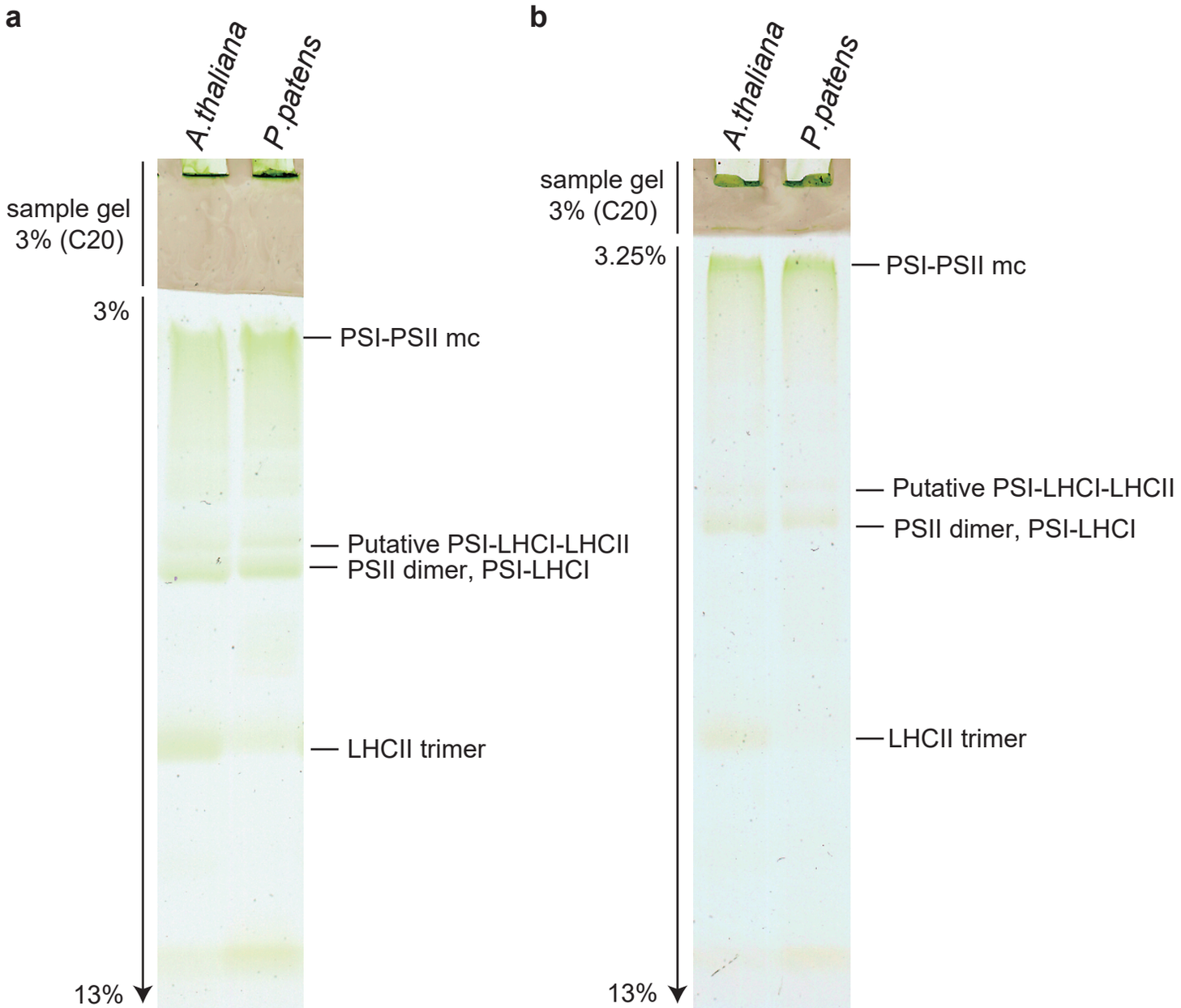

Furukawa et al.

Fig. 4

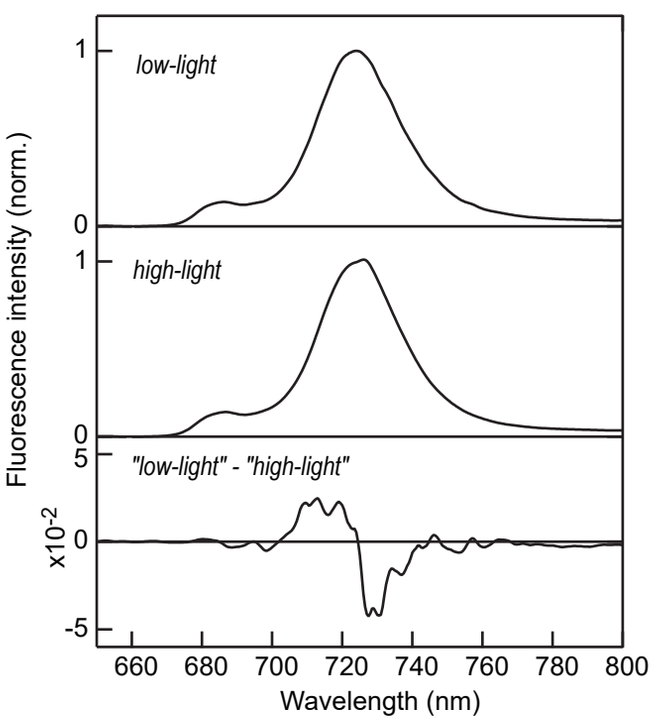
low-light
high-light
"low-light" - "high-light"
Fluorescence intensity (norm.)
x10-2
1
0
1
0
5
0
-5
660
680
700
720
740
760
780
800
Wavelength (nm)

Fig. 5

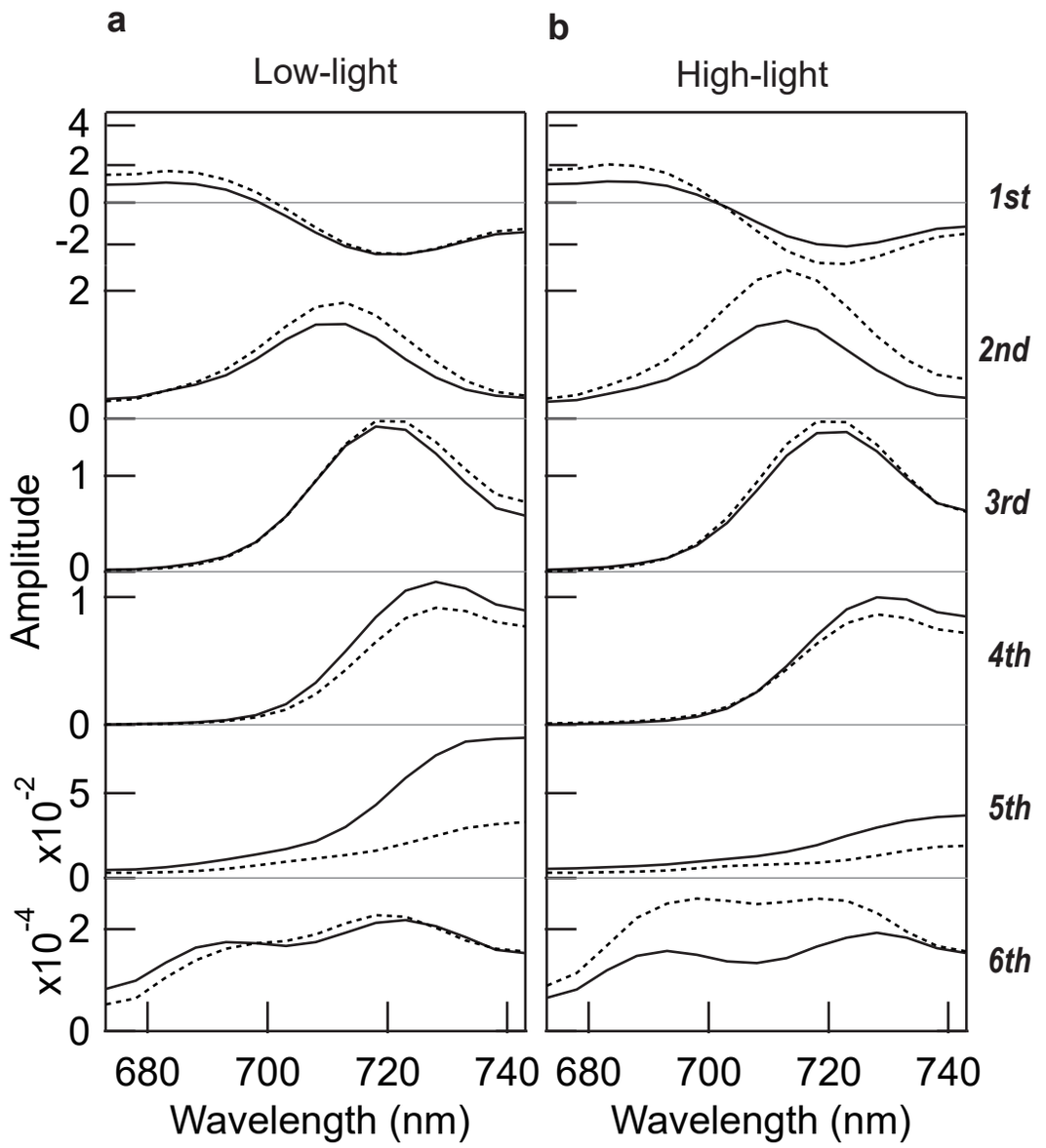

Furukawa et al.

Fig. 6

Arabidopsis thaliana

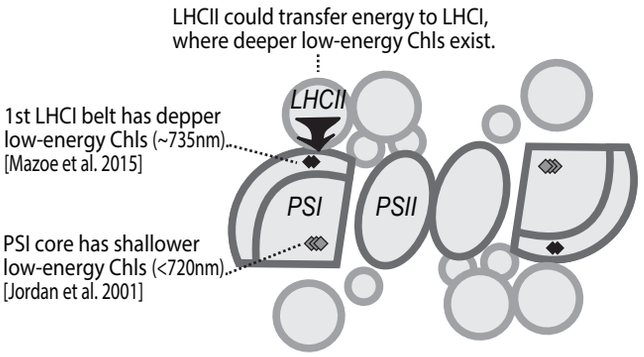

Physcomitrella patens

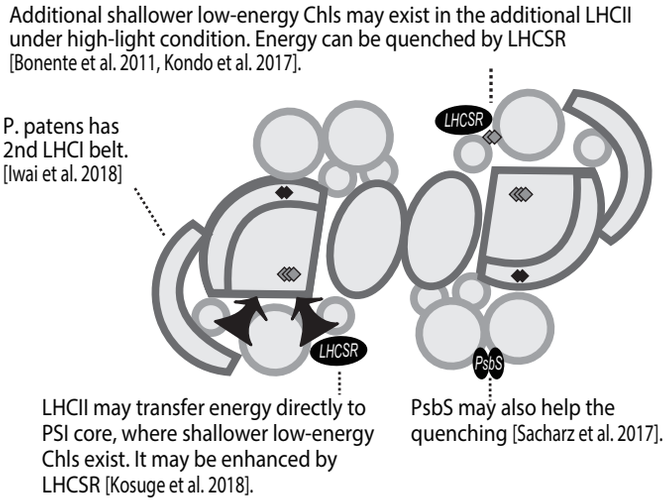

Furukawa et al.

Electronic supplementary materials

Title:

Formation of a PSI–PSII megacomplex containing LHCSR in the moss *Physcomitrella patens*

Authors:

Ryo Furukawa, Michiki Aso, Tomomichi Fujita, Seiji Akimoto, Ryouichi Tanaka, Ayumi Tanaka, Makio Yokono, and Atsushi Takabayashi

Journal:

Journal of Plant Research

Corresponding author:

Atsushi Takabayashi, Institute of Low Temperature Science, Hokkaido University, N19 W8 Kita-Ku, Sapporo 060-0819, Japan

(Affiliation, Address, Country)

TEL: +81-11-706-5493

E-mail: takabayashi@pop.lowtem.hokudai.ac.jp,

Co-Corresponding author:

Makio Yokono, Innovation Center, Nippon Flour Mills Co., Ltd., Atsugi 243-0041,

Japan

TEL: +81-80-3295-1623

E-mail: filia@mac.com,

Content:

Figs. S1–S9, Tables S1–S2

Fig. S1

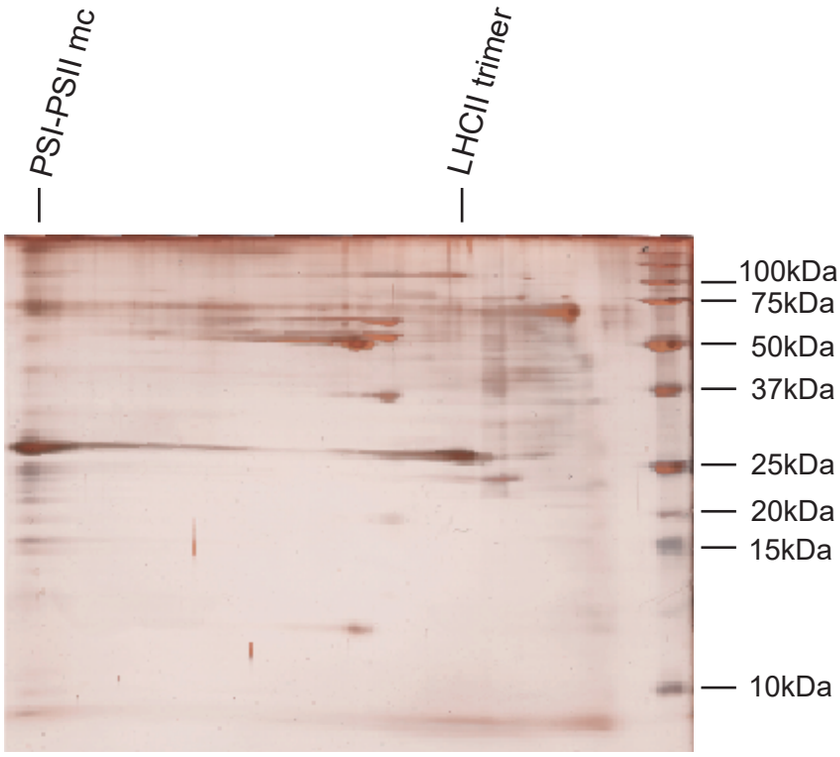

Fig. S1 Protein composition of the thylakoid protein complexes resolved by large-pore (lp) 2D-CN/SDS-PAGE. The 1D-lpCN-gel (3.5%–13%) used in this experiment is shown in Fig. 1. The proteins were visualized by silver-staining. The molecular mass markers are shown on the right-hand side of the gel. The positions of the corresponding bands on the lpCN-PAGE gel and their assignments are presented above the gel image.

Fig. S2

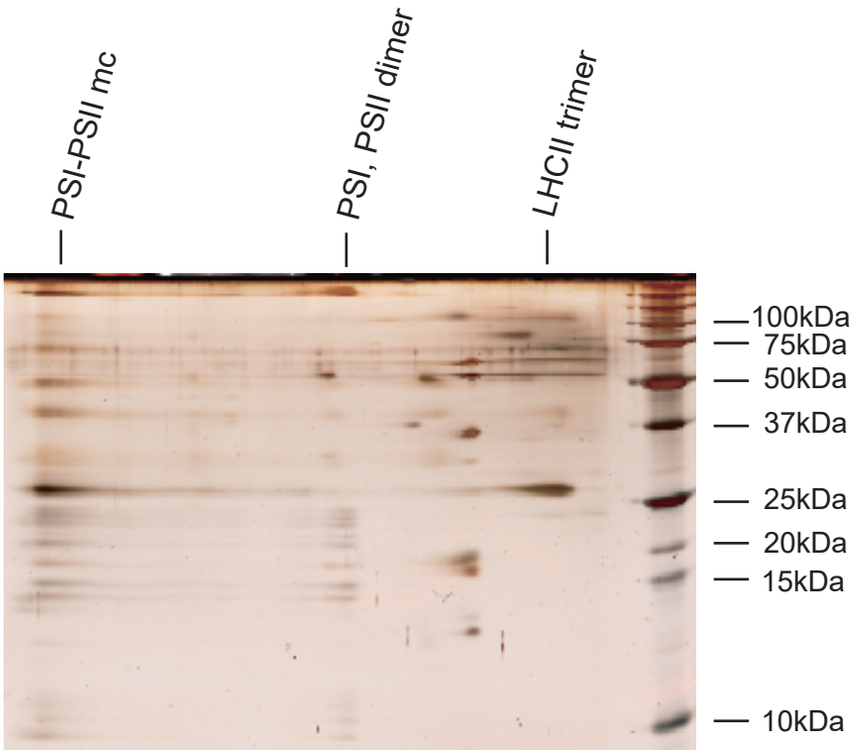

Fig. S2 Protein composition of the thylakoid protein complexes resolved by large-pore (lp) 2D-CN/SDS-PAGE. The 1D-lpCN-gel (3.25%–13%) used in this experiment is shown in Fig. 3 (B). The proteins were visualized by silver-staining. The molecular mass markers are shown on the right-hand side of the gel. The positions of the corresponding bands on the lpCN–PAGE gel and their assignments are presented above the gel image.

Fig. S3

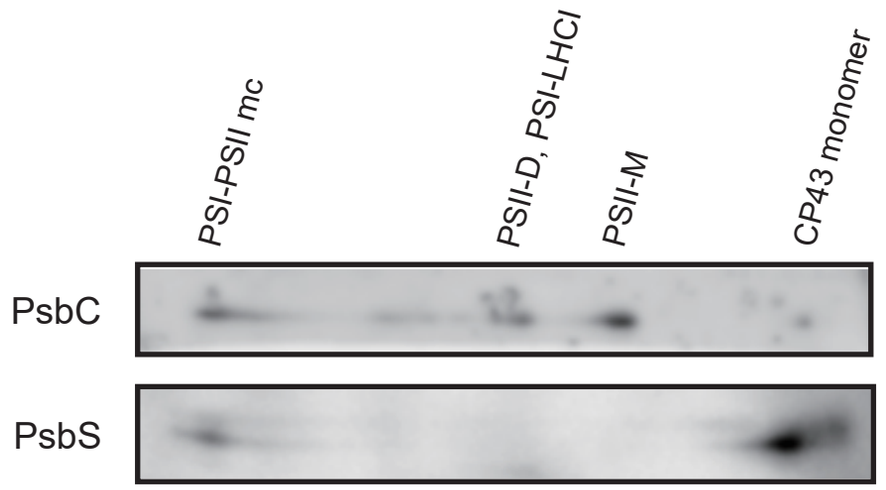

Fig. S3 Immunoblot analyses of PsbC (PSII) and PsbS proteins after 2D-lpCN/SDS-PAGE. The thylakoid protein complexes of low light grown cells were solubilized by 1% digitonin and resolved by the lpCN-PAGE (3.25%–13%), using amphipol A8-35 (Fig. 3B). Then, 2D-SDS-PAGE followed by immunoblot analysis with anti-PsbC antibodies and anti-PsbS antibodies, were performed.

Fig. S4

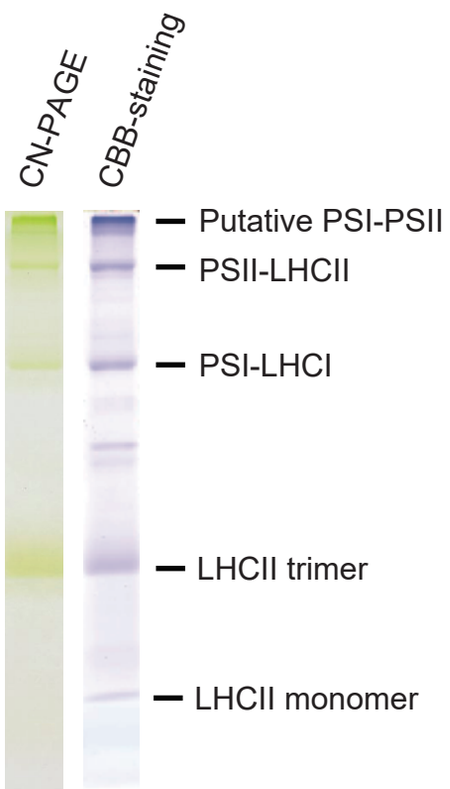

Fig. S4 Separation of pigment-protein complexes in *Physcomitrella* by CN-PAGE. Thylakoid membrane proteins were solubilized with 1% α-dodecyl maltoside and were separated by CN-PAGE with amphipol A8-35 using 4%–13% polyacrylamide.

Fig. S5

Time-resolved fluorescence spectra (raw spectra)

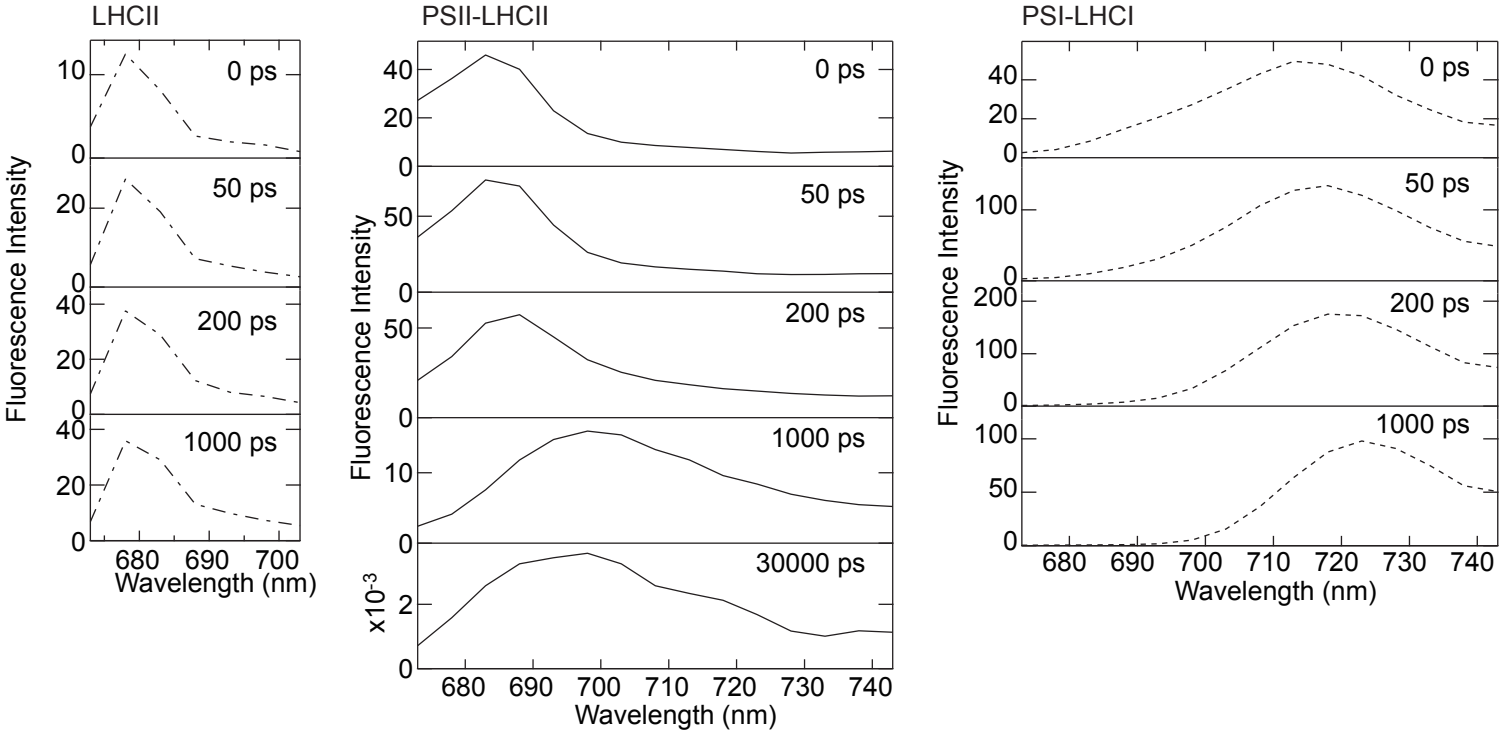

Re-constructed steady-state fluorescence spectra by integration on time axis

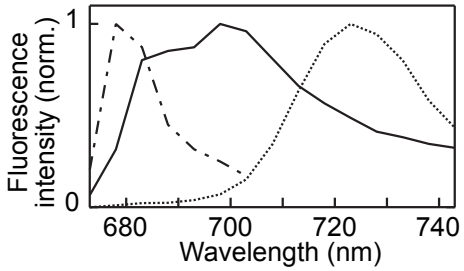

Fluorescence decay-associated spectra

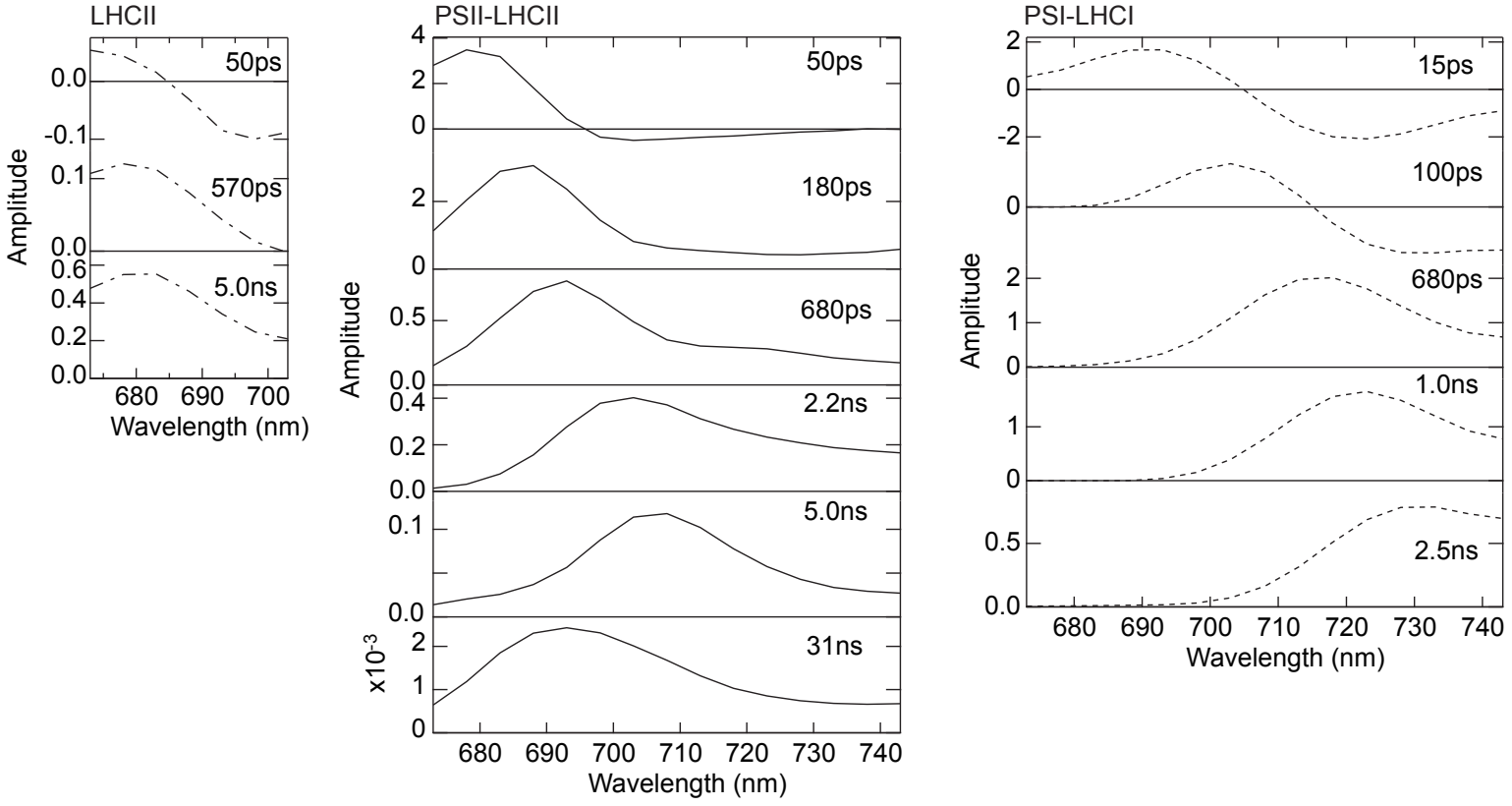

Fig. S5 77K fluorescence spectra of the PSI-LHCI, the PSII-LHCII, and the LHCII trimer resolved by CN-PAGE, after the solubilization of thylakoid membranes from the low light grown cells with 1% α-dodecyl maltoside. Upper, time-resolved fluorescence spectra (raw). Mid, re-constructed steady-state fluorescence spectra from the raw spectra. Lower, fluorescence decay-associated spectra.

Fig. S6

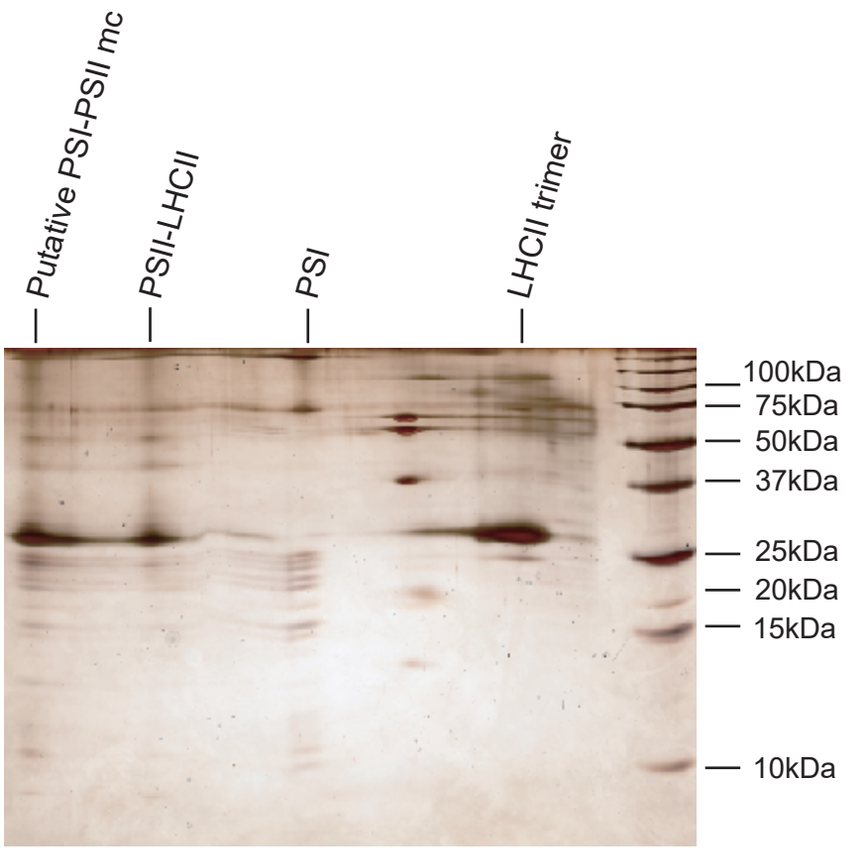

Fig. S6 Protein composition of the thylakoid protein complexes resolved by 2D-CN/SDS-PAGE followed by silver staining. The thylakoid protein complexes of low light grown cells were solubilized by 1% α-dodecyl maltoside. The solubilized protein complexes were firstly resolved by the CN-PAGE using amphipol A8-35 (Fig. S4) and then resolved by SDS-PAGE. The molecular mass markers are shown on the right-hand side of the gel. The positions of the corresponding bands on the CN-–PAGE gel and their assignments are presented above the gel image.

Fig. S7

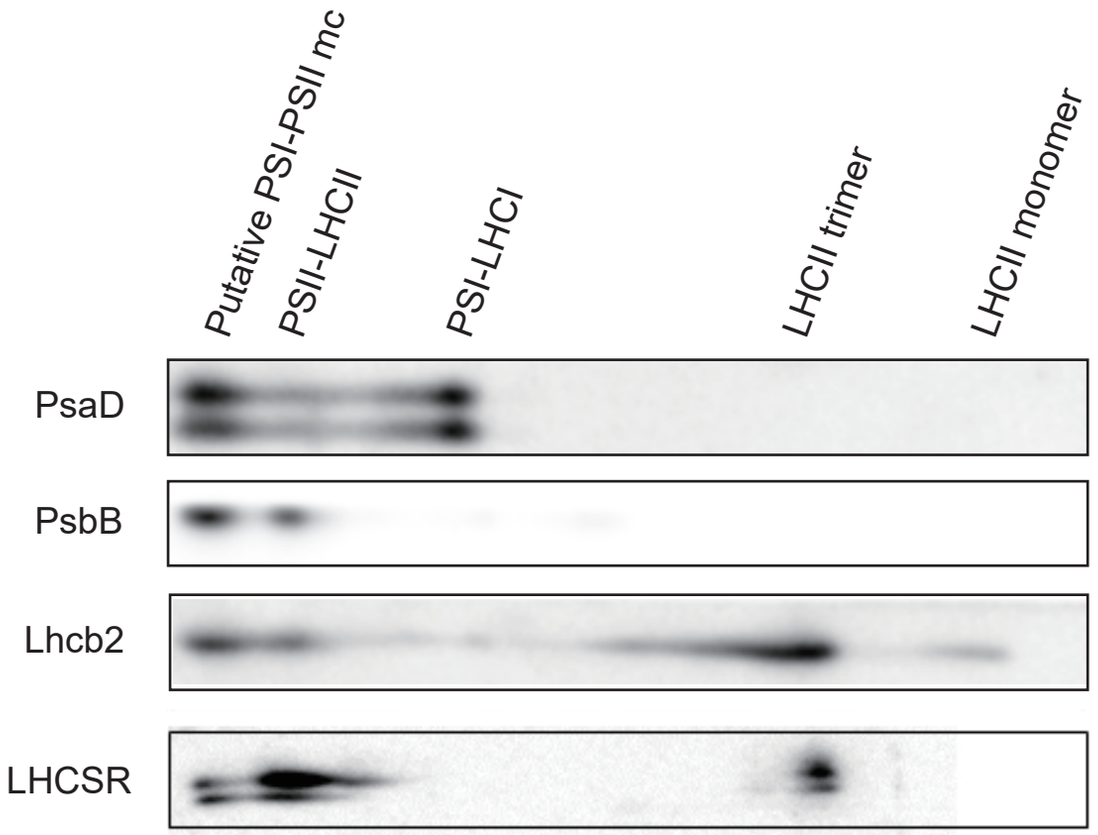

Fig. S7 Immunoblot analyses of PsaB (PSI), PsbB (PSII), Lhcb2 (LHCII), and LHCSR proteins after 2D-CN/SDS-PAGE. The thylakoid protein complexes of low light grown cells were solubilized by 1% α-dodecyl maltoside. The solubilized protein complexes were firstly resolved by the CN-PAGE using amphipol A8-35 (Fig. S4) and then resolved by SDS-PAGE.

Fig. S8

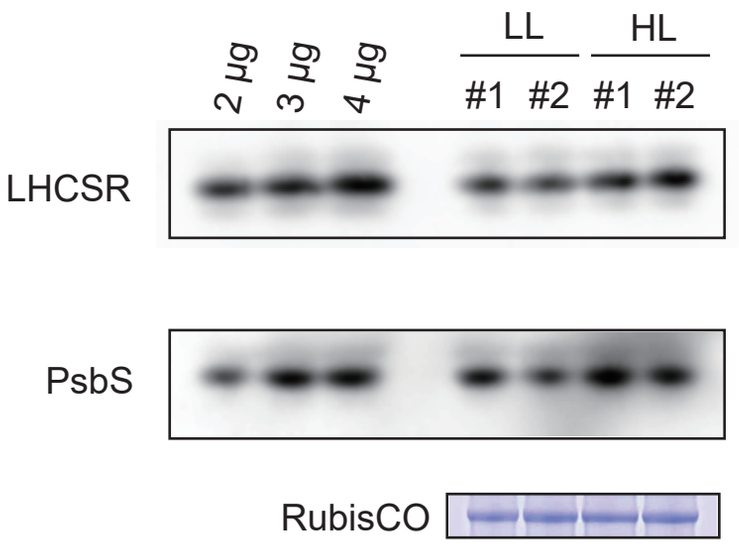

Fig. S8 Immunoblot analyses of LHCSR and PsbS proteins before and after 1 h strong light illumination. Whole cell proteins were extracted from the low light grown cells (LL) and the 1 h strong light illuminated cells (HL) and resolved by SDS-PAGE. Loading amounts (2 µg) of extracted proteins were estimated by XL-Bradford (APRO Science Inc., Tokyo, Japan) using the standard curve of BSA. The intensity of the CBB-stained RubisCO band was also used as the indication of the loading protein amount. Two biological replicates (#1 and #2) were used for LL and HL. A dilution series (2 µg , 3 µg, and 4 µg) of the LL sample (#1) was loaded.

Fig. S9

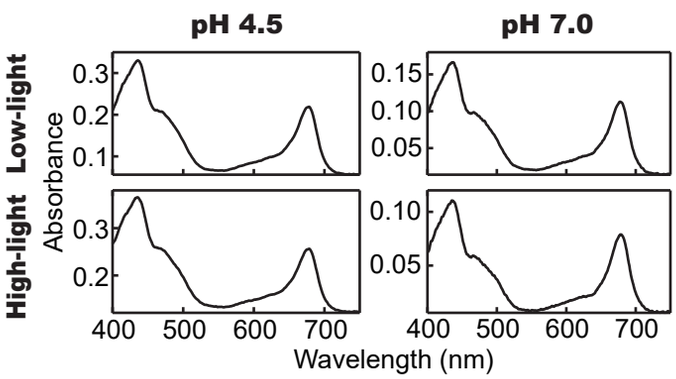

Fig. S9 Absorption spectra of the *Physcomitrella* PSI-PSII megacomplex measured at neutral pH (7.0) and low pH (4.5). The PSI-PSII megacomplex was solubilized from the *Physcomitrella* cells before and after 1 h strong light illumination and separated by lpCN-PAGE.

Table S1 Zeaxanthin levels before and after 1 h high light illumination

	LL	HL
Z / Chl *a* ratio	0.030 ± 0.011	0.123 ± 0.006
Z / VAZ ratio	0.171 ± 0.055	0.703 ± 0.010

Zeaxanthin (Z) content normalized by Chlorophyll (Chl) *a* or by total xanthophyll pigments (Violaxanthin (V), Antheraxanthin (A), and Z) before and after 1 h high light (HL) illumination of low light (LL) grown cells.

Table S2 Lifetimes of fluorescence decay-associated spectra of PSI-PSII megacomplex

	Low-light		**High-light**	
	pH7.0	**pH4.5**	**pH7.0**	**pH4.5**
	DNL1_7	**DNL1_4**	**DNH1_7**	**DNH1_4**
1st	45 ps	50 ps	50 ps	40 ps
2nd	200 ps	220 ps	230 ps	210 ps
3rd	750 ps	850 ps	860 ps	840 ps
4th	1.9 ns	2.1 ns	2.1 ns	2.1 ns
5th	4.1 ns	4.8 ns	4.9 ns	5.5 ns
6th	30 ns	25 ns	31 ns	25 ns
Mean Lifetime				
PSII: PSI (ns)	1.07: 1.46	0.90: 1.41	1.15: 1.47	0.95: 1.31
Delayed fluorescence Intensity (after vibrational band correction)				
PSII: PSI	0.183: 0.191	0.168: 0.216	0.163: 0.137	0.265: 0.226
Spillover ratio	43%	45%	40%	38%